Research Article

Fei Xie, Jinyuan Tang, Ailun Wang, Cijun Shuai, and Qingshan Wang*

Free vibration of functionally graded carbon nanotube reinforced composite cylindrical panels with general elastic supports

https://doi.org/10.1515/cls-2018-0008
Received Mar 31, 2018; accepted Apr 06, 2018

Abstract: In this paper, a unified solution for vibration analysis of the functionally graded carbon nanotube reinforced composite (FG-CNTRC) cylindrical panels with general elastic supports is carried out via using the Ritz method. The excellent accuracy and reliability of the present method are compared with the results of the classical boundary cases found in the literature. New results are given for vibration characteristics of FG-CNTRC cylindrical panels with various boundary conditions. The effects of the elastic restraint parameters, thickness, subtended angle and volume fraction of carbon nanotubes on the free vibration characteristic of the cylindrical panels are also reported.

Keywords: Cylindrical panels; Functionally graded carbon nanotube; Reinforced composite; Ritz method. General elastic supports

1 Introduction

Cylindrical panels as the common structural components have been widely applied in various engineering constructions, such as aircraft, space vehicles and structures of military industries. Therefore, the knowledge of vibration characteristics of the cylindrical panels is of particular importance for the predesign of the engineering structures. In most of these investigations studying the vibration behavior of the cylindrical panels, the boundary conditions taken into account are generally the perfect classical boundary cases, *i.e.* free, simply supported or clamped, however, in the real engineering application, the boundaries can be the general elastic supports and approximated by a combination of liner and rotational restraints. The objective of this paper is to present a first known free vibration solution for FG-CNT reinforced composite moderately thick cylindrical panels with general elastic supports.

Carbon nanotubes (CNTs) have extraordinary mechanical, electrical and thermal properties, and thus, they have attracted increasing attention in the past decades [1]. So far, a huge amount of research efforts on the vibrations of FG-CNT reinforced composite beams, plates and shells by using different methods and elastic theories have been made. Lin and Xiang [2] studied the linear free vibration of FG-CNT reinforced composite beams with classical boundary condition by using the *p*-Ritz method. The beam theory of this study was based on the first order and third order beam theories. Rafiee *et al.* [3] analyzed large amplitude free vibration of functionally graded carbon nanotube reinforced composite beams with surface-bonded piezoelectric layers based on the Euler–Bernoulli beam theory. Ke *et al.* [4] investigated the geometric nonlinear free vibration of FG-CNT beams based on the Timoshenko beam theory and von Kármán geometric nonlinearity. Later, Ke and his co-authors [5] considered the size effect and investigated the bending, buckling and vibration behavior of functionally graded micro plates. Shen [6] conducted the investigation on the nonlinear bending of simply supported FG-CNT reinforced composite plates by using a two-step perturbation technique. Zhu *et al.* [7] investigated the free vibration and static response of FG-CNT reinforced composite plates with classical boundary conditions by using the finite element method and first order shear deformation plate theory. Zhang *et al.* [8–10] used the element free methods to study the vibration characteristics of FG-CNT reinforced composite skew plates, triangular plates and cylindrical panels with classical boundary condition. In these researches, it is shown that, natural frequencies of plates and panels are affected by distribution pattern and volume fraction of CNTs. Malekzadeh and Zarei [11] ap-

***Corresponding Author: Qingshan Wang:** State Key Laboratory of High Performance Complex Manufacturing, Central South University, Changsha 410083, PR China; Email: wangqingshanxlz@hotmail.com; Tel.: +86-451-82519797
Fei Xie, Jinyuan Tang, Ailun Wang, Cijun Shuai: State Key Laboratory of High Performance Complex Manufacturing, Central South University, Changsha 410083, PR China

plied the differential quadrature method to examine the free vibration characteristics of laminated plates containing FG-CNT reinforced composite layers in an arbitrary straight-sided quadrilateral shape and arbitrary classical boundary conditions on the basis of the first order shear deformation plate theory. Later, Malekzadeh and Heydarpour [12] applied the mixed Navier-layerwise differential quadrature method to investigate the free vibration and static response of simply supported laminated plates with FG-CNTRC layers. Natarajan *et al.* [13] applied a higher order shear and normal deformable plate formulation to study the static and free vibrations of single layer FG-CNT reinforced composite plates and also sandwich plates with FG-CNT reinforced composite face sheets. Wang and Shen [14, 15] investigated the linear and nonlinear free vibrations of single layer FG-CNT reinforced composite plate and sandwich plates with stiff core and FG-CNT reinforced composite face sheets. In the researches, the interaction of the plate with two parameter elastic foundation is also taken into account. Shen [16] presented an investigation on the nonlinear dynamic response of FG-CNT reinforced composite resting on elastic foundations in thermal environments according to the von-Karman formulation and higher-order shear deformation theory. In this research, the solution method is the two-step perturbation technique and the boundary condition considered of the plate is all edges simply supported. Lei *et al.* [17] investigated the elastodynamics response of FG-CNT reinforced composite plates subjected to sudden lateral pressure by using element-free *kp*-Ritz method. Based on Reddy's third-order shear deformation theory, Zhang *et al.* [18] proposed a state space approach to study the free vibration characteristics of rectangular Levy plates with various classical boundary conditions. Zhang *et al.* [19] and Lei *et al.* [20] respectively studied the free vibration characteristics of FG-CNT reinforced composite plates with elastically restrained edges and laminated plates with FG-CNT reinforced composite layers. Liew and his co-authors [21–27] employed the element-free *kp*-Ritz method to study the vibration characteristic of the FG-CNT reinforced composite plates, *i.e.* buckling of skew FG-CNT reinforced composite plates, post-buckling of FG-CNT reinforced composite plates subjected to in-plane compressive loads, linear stress analysis of FG-CNT reinforced composite plates and so on. Mirzaei and Kiani [28] applied the Ritz method with Chebyshev polynomials to study the free vibration of FG-CNT reinforced composite reinforced composite cylindrical panels. In this research, the boundary condition was restricted to the classical boundary cases, *i.e.* CCCC, SCSF and so on. In addition to the above paper, a lot of critical research about the FG-CNTRC shells in recently has been published [29–38].

The above review indicates that there exists some literature on the vibration analysis of FG-CNT reinforced composite beams, plates and shells, and those numerical results are very useful for the practical engineering applications. However, from the literature review, we also know that the existing numerical solutions which are used to solve for the titled problem are very scarce. The only one study found in the published literature is about the vibration of moderately thick FG-CNT reinforced composite cylindrical panels with classical boundary conditions. Moreover, in practical engineering applications, the boundary condition of the FG-CNT reinforced composite cylindrical panels may not always be classical case in reality, and a variety of possible boundary conditions including classical boundary conditions, elastic boundary restraints and the combinations of two or more conditions may be encountered. As far as the authors know, there is no work reported on the free vibration behavior of FG-CNT reinforced composite cylindrical panels with general elastic supports based on first-order shear deformation theory. Thus, the establishment of a unified, efficient and accurate formulation for free vibration of FG-CNT reinforced composite cylindrical panels with general elastic supports is of crucial importance.

This paper attempts to provide a set of vibration frequencies for FG-CNT reinforced composite cylindrical panels of moderate thickness having general elastic supports. A enhanced Ritz method is presented based on the Ritz-variational energy method in conjunction with the modified Fourier series method. Compared with other methods, the proposed method can eliminate the limitations of the boundary conditions of the traditional Ritz method and be extended to the general boundary conditions. The first-order shear deformation theory (FSDT), accounting for transverse shear strains and rotary inertia, is used in the theoretical formulation. Based on the existing published literature, the present work can enrich the study for the practical engineering applications such as: (a) present a unified solution for vibration analysis of the moderately thick functionally graded carbon nanotube reinforced composite cylindrical panels with general elastic supports and (b) provide some useful numerical results for free vibration of thick open cylindrical shells with elastic boundary conditions and research conclusions for the influence of elastic restrain parameters, thickness, subtended angle and volume fraction of carbon nanotubes.

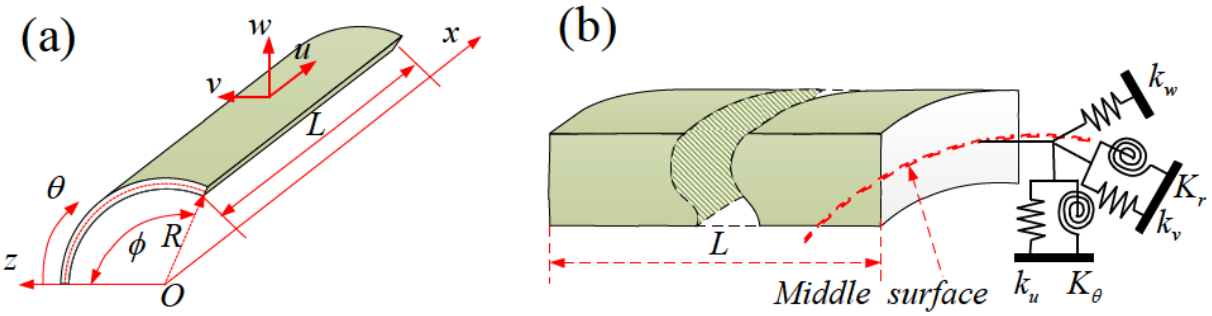

Figure 1: Geometry properties of FG-CNT reinforced composite cylindrical panel.

2 Theoretical formulations

2.1 Description of the model

The basic configuration of the problem considered here is a FG-CNT reinforced composite cylindrical panel as shown in Figure 1. A cylindrical coordinate system (x, θ, z) is also shown in the Figure 1(a), which will be used in the analysis. u, v and w denote the displacement components in x, θ and z directions. Length of the straight edge, radial, subtended angle and thickness of the FG-CNT reinforced composite cylindrical panel are assumed as L, R, ϕ, and h, respectively. As shown in Figure 1(b), three groups of liner restraint springs and two groups of rotation restraint springs are arranged at all sides of the cylindrical panels to separately simulate the general boundary condition. For example, the clamped boundary condition can be readily obtained by setting the spring coefficients to infinity (a very large number in practical calculation) for all restraint springs along each edge.

Polymeric matrix of the composite cylindrical panel is reinforced with single walled carbon nanotubes (SWCNTs) [28]. In this research, five types of aligned CNT reinforced cylindrical panels are considered: namely the uniformly distributed CNT cylindrical panel(UD-CNT), functionally graded CNT cylindrical panel type V(FGV-CNT) whose CNT features are concentrated at top region, functionally graded CNT cylindrical panel type Λ(FGΛ-CNT) whose CNT features are concentrated at bottom region, functionally graded CNT cylindrical panel type X(FGX-CNT) whose CNT features are concentrated at both top and bottom regions, and functionally graded CNT cylindrical panel type O(FGO-CNT) whose CNT features are concentrated at center regions, as shown in Figure 2. The reinforced CNT alignments are along the length direction, which is the x axis. For the above five CNT reinforced cylindrical panels, it is assumed that they will have the same geometries and contain the same value of total weight of CNTs m_{tcnt}, and with total CNTs volume fraction V_{tcnt}. For the latter four FG-CNT cylindrical panels, the CNT distributions along the thickness of the cylindrical panel follow the power laws, as shown in Figure 3.

Therefore the distribution of CNTs of FGΛ-CNT as a function of z coordinate is given by: [6]

$$f(z) = \left(\frac{h-2z}{2h}\right), \left(-\frac{h}{2} \le z \le \frac{h}{2}\right) \tag{1}$$

And the volume fraction of CNTs can be derived as

$$V_{CNT}(z) = (k+1)\left(\frac{h-2z}{2h}\right)^k V_{tcnt}, \left(-\frac{h}{2} \le z \le \frac{h}{2}\right) \tag{2}$$

However from the practical perspective, only the linear distribution is considered in the current study, *i.e.* $k = 1$

$$V_{CNT}(z) = \left(1 - \frac{2z}{h}\right) V_{tcnt}, \left(-\frac{h}{2} \le z \le \frac{h}{2}\right) \tag{3}$$

According to the same principle, the volume fraction of CNTs of the FGV-CNT, FGX-CNT, FGO-CNT and UD-CNT can be indicated as:

$$V_{CNT}(z) = \begin{cases} \left(1 + \frac{2z}{h}\right) V_{tcnt}\,(\mathrm{FGV-CNT}) \\ 4\frac{|z|}{h} V_{tcnt}\,(\mathrm{FGX-CNT}) \\ 2\left(1 - 2\frac{|z|}{h}\right) V_{tcnt}\,(\mathrm{FGO-CNT}) \\ V_{tcnt}\,(\mathrm{UD-CNT}) \end{cases} \quad \left(-\frac{h}{2} \le z \le \frac{h}{2}\right) \tag{4}$$

The effective Young's modulus and shear modulus of the CNT composite cylindrical panel are determined based on matching the results from the molecular dynamics simulation with the extended rule of mixture. The expressions are as follows [6]:

$$E_{11}(z) = \eta_1 V_{CNT}(z) E_{11}^{cnt} + V_m(z) E^m \tag{5a}$$

$$\frac{\eta_2}{E_{22}(z)} = \frac{V_{CNT}(z)}{E_{22}^{cnt}} + \frac{V_m(z)}{E^m} \tag{5b}$$

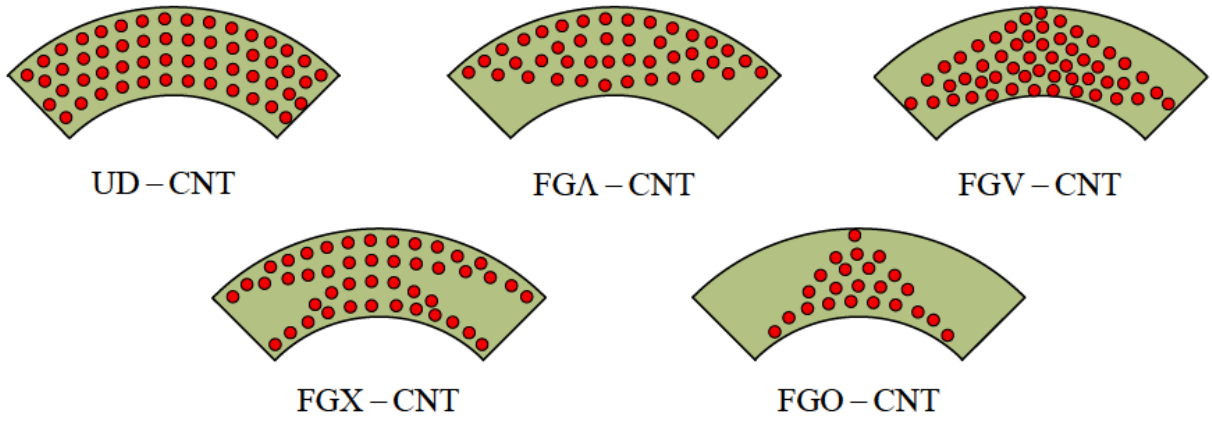

Figure 2: Distribution types of CNTs of FG-CNT reinforced composite panels.

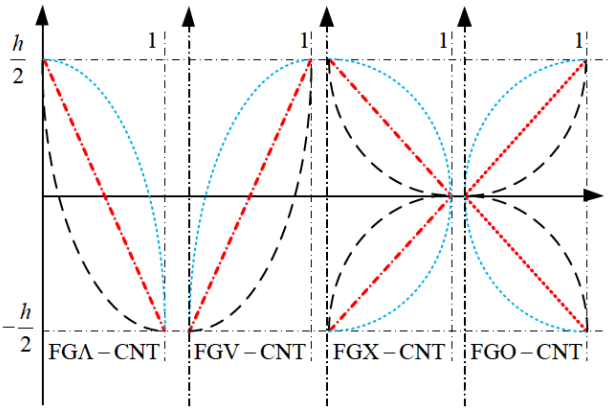

Figure 3: CNT distribution shape function of FG-CNT reinforced composite panels.

$$\frac{\eta_3}{G_{12}(z)} = \frac{V_{CNT}(z)}{G_{12}^{cnt}} + \frac{V_m(z)}{G^m} \tag{5c}$$

$$\mu_{12}(z) = V_{CNT}(z)\,\mu_{12}^{cnt} + V_m(z)\,\mu^m \tag{5d}$$

$$\mu_{21}(z) = \frac{\mu_{12}(z)}{E_{11}(z)} E_{22}(z) \tag{5e}$$

$$\rho(z) = V_{CNT}(z)\,\rho^{cnt} + V_m(z)\,\rho^m \tag{5f}$$

$$V_m(z) = 1 - V_{CNT}(z) \tag{5g}$$

where E_{11}^{cnt}, E_{22}^{cnt}, G_{12}^{cnt}, E^m and G^m are Young's modulus and shear modulus of CNT and matrix, η_1, η_2 and η_3 are CNT/matrix efficiency parameters, μ_{12}^{cnt} and μ^m are Poisson's ratios of CNT and matrix, and ρ^{cnt} and ρ^m are the mass densities of CNT and matrix constituents, respectively.

2.2 Total energy functional

According to the FSDT assumptions, the displacement components of an arbitrary point in the FG-CNT reinforced composite cylindrical panel are expressed in terms of the displacements and rotations of the reference surface, as given below [28]:

$$u(x,\theta,z,t) = u_0(x,\theta,t) + z\psi_x(x,\theta,t) \tag{6a}$$

$$v(x,\theta,z,t) = v_0(x,\theta,t) + z\psi_\theta(x,\theta,t) \tag{6b}$$

$$w(x,\theta,z,t) = w_0(x,\theta,t) \tag{6c}$$

where u_0, v_0 and w_0 denote the displacements of the corresponding point on the reference surface in the x, θ and z directions, respectively. ψ_x and ψ_θ are the rotations of the normal to the reference surface about the θ and x direction, respectively, and t is the time. The strains in the middle surface and curvature changes during deformation for a FG-CNT reinforced composite cylindrical panel having constant radius R are defined as

$$\varepsilon_x^0 = \frac{\partial u_0}{\partial x}, \quad \varepsilon_\theta^0 = \frac{1}{R}\frac{\partial v_0}{\partial \theta} + \frac{w_0}{R}, \quad \gamma_{x\theta}^0 = \frac{\partial v_0}{\partial x} + \frac{\partial u_0}{R\partial\theta}, \quad \kappa_x = \frac{\partial \psi_x}{\partial x}, \quad \kappa_\theta = \frac{\partial \psi_\theta}{R\partial\theta}, \quad \kappa_{x\theta} = \frac{\partial \psi_\theta}{\partial x} + \frac{\partial \psi_x}{R\partial\theta} \tag{7}$$

where the ε_x^0, ε_θ^0 and $\gamma_{x\theta}^0$ denote the strains in the middle surface. κ_x, κ_θ and $\kappa_{x\theta}$ are the curvature changes. The liner strain–displacement relations of the FG-CNT reinforced composite cylindrical panel are defined as

$$\varepsilon_{xx} = \varepsilon_x^0 + z\kappa_x, \quad \varepsilon_{\theta\theta} = \varepsilon_\theta^0 + z\kappa_\theta, \quad \gamma_{x\theta} = \gamma_{x\theta}^0 + z\kappa_{x\theta}, \quad \gamma_{xz} = \frac{\partial w_0}{\partial x} + \psi_x, \quad \gamma_{\theta z} = \frac{\partial w_0}{R\partial\theta} - \frac{v_0}{R} + \psi_\theta \tag{8}$$

According to general Hooke's law, the corresponding stresses are obtained as:

$$\begin{Bmatrix}\sigma_{xx}\\ \sigma_{\theta\theta}\\ \tau_{\theta z}\\ \tau_{xz}\\ \tau_{x\theta}\end{Bmatrix} = \begin{bmatrix}Q_{11} & Q_{12} & 0 & 0 & 0\\ Q_{12} & Q_{22} & 0 & 0 & 0\\ 0 & 0 & Q_{44} & 0 & 0\\ 0 & 0 & 0 & Q_{55} & 0\\ 0 & 0 & 0 & 0 & Q_{55}\end{bmatrix} \begin{Bmatrix}\varepsilon_{xx}\\ \varepsilon_{\theta\theta}\\ \gamma_{\theta z}\\ \gamma_{xz}\\ \gamma_{x\theta}\end{Bmatrix} \quad (9)$$

where Q_{ij} (i, j=1, 2, 4, 5, 6) are the reduced material stiffness coefficients compatible with the plane-stress conditions and are obtained as follows

$$Q_{11} = \frac{E_{11}}{1-\mu_{12}\mu_{21}}, \quad Q_{22} = \frac{E_{22}}{1-\mu_{12}\mu_{21}}, \quad (10)$$
$$Q_{12} = \frac{\mu_{21}E_{11}}{1-\mu_{12}\mu_{21}}, \quad Q_{44} = G_{23}, Q_{55} = G_{13}, Q_{66} = G_{12}$$

By carrying the integration of stresses over the cross-section and integrating the moments of the in-plane stresses over the thickness, the force and moment resultants to strains and curvatures of the reference surface are given in the matrix form:

$$\begin{bmatrix}N_x\\ N_\theta\\ N_{x\theta}\\ M_x\\ M_\theta\\ M_{x\theta}\end{bmatrix} = \begin{bmatrix}A_{11} & A_{12} & 0 & B_{11} & B_{12} & 0\\ A_{12} & A_{22} & 0 & B_{12} & B_{22} & 0\\ 0 & 0 & A_{66} & 0 & 0 & B_{66}\\ B_{11} & B_{12} & 0 & D_{11} & D_{12} & 0\\ B_{12} & B_{22} & 0 & D_{12} & D_{22} & 0\\ 0 & 0 & B_{66} & 0 & 0 & D_{66}\end{bmatrix} \begin{bmatrix}\varepsilon_x^0\\ \varepsilon_\theta^0\\ \gamma_{x\theta}^0\\ \kappa_x\\ \kappa_\theta\\ \kappa_{x\theta}\end{bmatrix} \quad (11)$$
$$\begin{bmatrix}Q_x\\ Q_\theta\end{bmatrix} = \begin{bmatrix}\kappa A_{66} & 0\\ 0 & \kappa A_{66}\end{bmatrix} \begin{bmatrix}\gamma_{xz}\\ \gamma_{\theta z}\end{bmatrix}$$

where N_x, N_θ and N_{theta} are the in-plane force resultants, M_x, M_θ and $M_{x\theta}$ are moment resultants, Q_x, Q_θ are transverse shear force resultants. κ is the shear correction factor, which is usually selected as $\kappa = 5/6$. A_{ij}, B_{ij} and D_{ij} (i,j = 1,2 and 6) are the extensional, extensional-bending coupling, bending stiffness, and they are respectively expressed as

$$(A_{ij}, B_{ij}, D_{ij}) = \int_{-h/2}^{h/2} Q_{ij}(z)(1, z, z^2)dz \quad (12)$$

The strain energy (U_S) of the moderately thick FG-CNT reinforced composite cylindrical panel during vibration can be defined as:

$$U_S = \frac{1}{2}\int\int\int_V \begin{Bmatrix} N_x\varepsilon_x^0 + N_\theta\varepsilon_\theta^0 + N_{x\theta}\gamma_{x\theta}^0\\ +M_x\kappa_x + M_\theta\kappa_\theta + M_{x\theta}\kappa_{x\theta}\\ +Q_x\gamma_{xz} + Q_y\gamma_{\theta z}\end{Bmatrix} dV \quad (13)$$

Substituting Eqs. (7), (8) and (11) into Eq. (9), the strain energy expression of the structure can be written in terms of middle surface displacements and rotations.

$$U = \frac{1}{2}\int\int_S \begin{Bmatrix} A_{11}\left(\frac{\partial u_0}{\partial x}\right)^2 + A_{22}\left(\frac{1}{R}\frac{\partial v_0}{\partial\theta} + \frac{w_0}{R}\right)^2\\ +A_{66}\left(\frac{\partial v_0}{\partial x} + \frac{\partial u_0}{R\partial\theta}\right)^2 + \kappa A_{66}\left(\frac{\partial w_0}{\partial x} + \psi_x\right)^2\\ +\kappa A_{66}\left(\frac{\partial w_0}{R\partial\theta} - \frac{v_0}{R} + \psi_\theta\right)^2\\ +2A_{12}\left(\frac{\partial u_0}{\partial x}\right)\left(\frac{1}{R}\frac{\partial v_0}{\partial\theta} + \frac{w_0}{R}\right)\\ +2B_{11}\frac{\partial u_0}{\partial x}\frac{\partial\psi_x}{\partial x} + B_{22}\left(\frac{1}{R}\frac{\partial v_0}{\partial\theta} + \frac{w_0}{R}\right)\frac{\partial\psi_\theta}{R\partial\theta}\\ +2B_{12}\frac{\partial u_0}{\partial x}\frac{\partial\psi_\theta}{R\partial\theta} + 2B_{12}\left(\frac{1}{R}\frac{\partial v_0}{\partial\theta} + \frac{w_0}{R}\right)\frac{\partial\psi_x}{\partial x}\\ +2B_{66}\left(\frac{\partial v_0}{\partial x} + \frac{\partial u_0}{R\partial\theta}\right)\left(\frac{\partial\psi_\theta}{\partial x} + \frac{\partial\psi_\theta}{R\partial\theta}\right)\\ +D_{11}\left(\frac{\partial\psi_x}{\partial x}\right)^2 + D_{22}\left(\frac{\partial\psi_\theta}{R\partial\theta}\right)^2\\ +2D_{12}\left(\frac{\partial\psi_x}{\partial x}\right)\left(\frac{\partial\psi_\theta}{R\partial\theta}\right) + D_{66}\left(\frac{\partial\psi_\theta}{\partial x} + \frac{\partial\psi_x}{R\partial\theta}\right)^2\end{Bmatrix} \quad (14)$$

The corresponding kinetic energy (T) function of the moderately thick FG-CNT reinforced composite cylindrical panel can be given as:

$$T = \frac{1}{2}\int\int_S \begin{Bmatrix} I_0\left[\left(\frac{\partial u_0}{\partial t}\right)^2 + \left(\frac{\partial v_0}{\partial t}\right)^2 + \left(\frac{\partial w_0}{\partial t}\right)^2\right]\\ +2I_1\left(\frac{\partial u_0}{\partial t}\frac{\partial\psi_x}{\partial t} + \frac{\partial v_0}{\partial t}\frac{\partial\psi_\theta}{\partial t}\right)\\ +I_2\left[\left(\frac{\partial\psi_x}{\partial t}\right)^2 + \left(\frac{\partial\psi_\theta}{\partial t}\right)^2\right]\end{Bmatrix} dS \quad (15)$$

where

$$\begin{pmatrix} I_0 & I_1 & I_2\end{pmatrix} = \int_{-h/2}^{h/2}\rho(z)\left(1, z^1, z^2\right)dz \quad (16)$$

The potential energy U_{sp} stored in the boundary springs is given as:

$$U_{sp} = \frac{1}{2}\int_{-\frac{h}{2}}^{\frac{h}{2}}\int_0^{\phi} \begin{Bmatrix}\left[k_{x0}^u u_0^2 + k_{x0}^v v_0^2\right.\\ \left.+k_{x0}^w w_0^2 + K_{x0}^x\psi_x^2 + K_{x0}^\theta\psi_\theta^2\right]_{x=0}\\ \left[k_{x1}^u u_0^2 + k_{x1}^v v_0^2\right.\\ \left.+k_{x1}^w w_0^2 + K_{x1}^x\psi_x^2 + K_{x1}^\theta\psi_\theta^2\right]_{x=L}\end{Bmatrix} Rd\theta dz \quad (17)$$

$$+\frac{1}{2}\int_{-\frac{h}{2}}^{\frac{h}{2}}\int_0^{L} \begin{Bmatrix}\left[k_{\theta0}^u u_0^2 + k_{\theta0}^v v_0^2\right.\\ \left.+k_{\theta0}^w w_0^2 + K_{\theta0}^x\psi_x^2 + K_{\theta0}^\theta\psi_\theta^2\right]_{\theta=0}\\ \left[k_{\theta1}^u u_0^2 + k_{\theta1}^v v_0^2\right.\\ \left.+k_{\theta1}^w w_0^2 + K_{\theta1}^\alpha\psi_x^2 + K_{\theta1}^\beta\psi_\theta^2\right]_{\theta=\phi}\end{Bmatrix} dxdz$$

Therefore, the total energy functional for the FG-CNT reinforced composite cylindrical panel can be expressed as:

$$\prod = T - U_S - U_{SP} \quad (18)$$

2.3 The Ritz method

Because of its simplicity and high accuracy, the Ritz method is widely used in the vibration analysis of struc-

tural elements as a very powerful tool. In the Ritz method, the solutions can be obtained by minimizing the energy functional with respect to the coefficients of the admissible functions. So how to choose the proper admissible functions is the core of study, for it plays the biggest factor in determining the accuracy and stability of the Ritz method. When it comes to the admissible functions, there are two conditions that should be satisfied in Ritz method. Firstly, the admissible functions should be continuous, linearly independent, complete and differentiable to the degree. Secondly, they should satisfy at least the geometrical boundary conditions [39]. Since the geometrical boundary conditions can be easily satisfied by setting the proper springs' stiffness in this work, any linearly independent and complete basis functions may be employed. In this paper, a modified Fourier series [40–60] is introduced to express the displacement and rotation components of the composite beams. The modified Fourier series consists of a standard Fourier cosine series and several auxiliary functions. Here, the introduction of the auxiliary functions is to remove the discontinuities potentially exhibited by the original displacement functions and their derivatives. And it also can accelerate the convergence of the representations at the same time. The detailed expressions of the displacement and rotation components are given as:

$$\begin{Bmatrix} u_0 \\ v_0 \\ w_0 \\ \psi_x \\ \psi_\theta \end{Bmatrix} = \sum_{m=0}^{M}\sum_{n=0}^{N} \begin{Bmatrix} A_{mn}^u \\ B_{mn}^v \\ C_{mn}^w \\ D_{mn}^x \\ E_{mn}^\theta \end{Bmatrix} \cos\lambda_m x \cos\lambda_n \theta + \sum_{l=1}^{2} \chi_l(\theta) \sum_{m=0}^{M} \begin{Bmatrix} a_m^l \\ c_m^l \\ e_m^l \\ g_m^l \\ k_m^l \end{Bmatrix} \cos\lambda_m x + \sum_{l=1}^{2} \zeta_l(x) \sum_{n=0}^{N} \begin{Bmatrix} b_n^l \\ d_n^l \\ f_n^l \\ h_n^l \\ q_n^l \end{Bmatrix} \cos\lambda_n \theta \tag{19}$$

where $\lambda_m = m\pi/L$, $\lambda_n = n\pi/\phi$, and A_{mn}^u, B_{mn}^v, C_{mn}^w, D_{mn}^x, E_{mn}^θ are the Fourier coefficients of two-dimensional Fourier series expansions for the displacements functions, respectively. a_m^l, b_n^l, c_m^l, d_n^l, e_m^l, f_n^l, g_m^l, h_n^l, k_m^l, q_n^l are the supplemented coefficients of the auxiliary functions $\chi_l(\theta)$ and $\zeta_l(x)$, where $l = 1, 2$. The two types of auxiliary functions $\chi_l(\theta)$ and $\zeta_l(x)$ are selected to remove all the discontinuities potentially associated with the first-order derivatives at the boundaries. Thus, the function sets are capable of representing any free vibration motion of the shell. The two types of auxiliary functions are given as:

$$\zeta(x) = \begin{cases} \zeta_1(x) = \frac{L}{2\pi}\sin\left(\frac{\pi x}{2L}\right) + \frac{L}{2\pi}\sin\left(\frac{3\pi x}{2L}\right) \\ \zeta_2(x) = -\frac{L}{2\pi}\cos\left(\frac{\pi x}{2L}\right) + \frac{L}{2\pi}\cos\left(\frac{3\pi x}{2L}\right) \end{cases} \tag{20a}$$

$$\chi(\theta) = \begin{cases} \chi_1(\theta) = \frac{\phi}{2\pi}\sin\left(\frac{\pi\theta}{2\phi}\right) + \frac{\phi}{2\pi}\sin\left(\frac{3\pi\theta}{2\phi}\right) \\ \chi_2(\theta) = -\frac{\phi}{2\pi}\cos\left(\frac{\pi\theta}{2\phi}\right) + \frac{\phi}{2\pi}\cos\left(\frac{3\pi\theta}{2\phi}\right) \end{cases} \tag{20b}$$

It is easy to verify that

$$\zeta_1(0) = \zeta_1(L) = \zeta_1'(L) = 0, \zeta_1'(0) = 1 \tag{21a}$$

$$\zeta_2(0) = \zeta_2(L) = \zeta_2'(0) = 0, \zeta_2'(L) = 1 \tag{21b}$$

$$\chi_1(0) = \chi_1(\phi) = \chi_1'(\phi) = 0, \chi_1'(0) = 1 \tag{21c}$$

$$\chi_2(0) = \chi_2(\phi) = \chi_2'(0) = 0, \chi_2'(\phi) = 1 \tag{21d}$$

The above equation (19) has constructed the admissible functions of the panels, the following task is to determine the coefficients of the admissible functions. Substituting Eq. (19) into Eq. (18) and performing the Ritz procedure with respect to each unknown coefficient:

$$\frac{\partial \prod}{\partial \iota} = 0, \iota = A_{mn}^u, a_m^l, b_n^l, B_{mn}^v, c_m^l, d_n^l, \cdots E_{mn}^\theta, g_m^l, h_n^l \tag{22}$$

the equations of motion for FG-CNT reinforced composite cylindrical panel can be yielded and are given in the matrix form:

$$\left(\mathbf{K} - \omega^2 \mathbf{M}\right)\mathbf{H} = \mathbf{0} \tag{23}$$

where **K**, **M** and **H** respectively represent the stiffness matrix, mass matrix and vector of the unknown coefficients for the panel and shell. The detail expressions for above matrices are given in Appendix. By solving the Eq. (23), the frequencies (or eigenvalues) of moderately thick FG-CNT reinforced composite cylindrical panel can be readily obtained and the mode shapes can be yielded by substituting the corresponding eigenvectors into series representations of displacement components.

3 Numerical results and discussion

The aim of this paper is to present a unified solution for vibration analysis of the moderately thick functionally graded carbon nanotube reinforced composite cylindrical

Table 1: The corresponding elastic restraint parameters for various boundary conditions.

BC	x=constant					θ=constant				
	Γ_u	Γ_v	Γ_w	Γ_x	Γ_θ	Γ_u	Γ_v	Γ_w	Γ_r	Γ_θ
F	0	0	0	0	0	0	0	0	0	0
C	10^{15}	10^{15}	10^{15}	10^{15}	10^{15}	10^{15}	10^{15}	10^{15}	10^{15}	10^{15}
S	10^{15}	10^{15}	10^{15}	0	10^{15}	10^{15}	10^{15}	10^{15}	10^{15}	0
SD	0	10^{15}	10^{15}	0	10^{15}	10^{15}	0	10^{15}	10^{15}	0
E^1	10^9	10^{15}	10^{15}	10^{15}	10^{15}	10^9	10^{15}	10^{15}	10^{15}	10^{15}
E^2	10^{15}	10^9	10^{15}	10^{15}	10^{15}	10^{15}	10^9	10^{15}	10^{15}	10^{15}
E^3	10^9	10^9	10^{15}	10^{15}	10^{15}	10^9	10^9	10^{15}	10^{15}	10^{15}

Table 2: Comparison of the frequency parameters Ω for a FG-CNT reinforced composite panel with CCCC boundary condition.

V^*_{tcn}	Mode	Ref [28]					Prsent Method				
		UD-CNT	FGX-CNT	FGO-CNT	FGV-CNT	FGΛ-CNT	UD-CNT	FGX-CNT	FGO-CNT	FGV-CNT	FGΛ-CNT
0.12	1	30.8185	32.3134	28.2171	29.3736	29.5779	30.7740	32.2626	28.1646	29.3426	29.5029
	2	31.0872	32.6868	28.5113	29.9670	29.8751	30.9663	32.5596	28.3725	29.8541	29.7091
	3	43.6652	45.4421	41.4832	42.9944	43.0527	43.4978	45.2510	41.2976	42.8173	42.8428
	4	55.2600	57.5570	50.8519	52.8115	53.1919	55.2412	57.5319	50.8305	52.8247	53.1289
	5	56.1307	58.4187	51.9473	54.1355	54.0803	56.0636	58.3411	51.8716	54.1061	53.9447
	6	59.8947	61.9304	57.9319	59.6789	59.7610	59.6886	61.6777	57.7152	59.4751	59.4881
0.17	1	39.1149	41.3499	35.6791	37.2313	37.5507	39.0593	41.2807	35.6013	37.1968	37.4360
	2	39.5288	42.0579	35.9702	38.0917	38.0358	39.3731	41.8892	35.7723	37.9412	37.7972
	3	55.9735	59.0921	52.7775	55.2537	55.4066	55.7581	58.8325	52.5018	55.0016	55.1078
	4	70.2537	73.7120	64.2459	66.9549	67.5400	70.2370	73.6832	64.2174	66.9952	67.4400
	5	71.4682	75.0173	65.6856	68.7939	68.8342	71.3880	74.9188	65.5812	68.7757	68.6321
	6	77.1109	80.9662	73.9916	77.0830	77.3306	76.8472	80.6177	73.6637	76.7952	76.9375
0.28	1	42.7465	45.7199	39.3330	41.5170	41.8735	42.6888	45.6367	39.1486	41.5018	41.7403
	2	43.0013	46.8451	39.7567	42.0378	42.2769	42.8438	46.6462	39.6820	41.9111	42.0157
	3	59.7374	65.6277	55.6951	59.7384	60.1538	59.5151	65.3093	55.4326	59.4785	59.8651
	4	76.4467	81.0748	71.9678	74.6099	75.2287	76.4263	81.0296	71.9467	74.6925	75.0982
	5	77.4735	82.6147	72.8186	76.0233	76.4855	77.3905	82.4844	72.7372	76.0783	76.2387
	6	81.4506	89.6000	76.6886	82.3614	83.1103	81.1754	89.1644	76.3819	82.0915	82.7324

Table 3: Comparison of the frequency parameters Ω for a FG-CNT reinforced composite panel with SSSS boundary condition.

V^*_{tcn}	Mode	Ref [28]					Prsent Method				
		UD-CNT	FGX-CNT	FGO-CNT	FGV-CNT	FGΛ-CNT	UD-CNT	FGX-CNT	FGO-CNT	FGV-CNT	FGΛ-CNT
0.12	1	21.4707	23.2763	19.1857	21.2857	21.2174	21.3072	23.1197	18.9935	21.1334	21.1231
	2	24.2713	25.9075	22.2689	24.0223	24.1057	24.2177	25.8532	22.2002	23.9828	24.0262
	3	32.8539	34.6039	31.0633	32.9915	32.7165	32.6632	34.4034	30.8477	32.8039	32.4869
	4	48.9129	50.9478	43.7103	46.4638	46.5784	48.6342	50.6337	43.6241	46.4825	46.4384
	5	50.0057	53.5101	43.7962	46.7978	47.0623	49.9364	53.4372	43.7717	46.7621	46.9920
	6	50.3795	53.9976	47.1745	48.9821	49.2402	50.3593	53.9735	46.8776	48.6914	48.9216
0.17	1	27.0580	29.5672	24.1626	26.9125	26.8335	26.8431	29.3602	23.8959	26.7135	26.5611
	2	30.7096	32.8979	28.3325	30.4933	30.5959	30.6399	32.8233	28.2274	30.4444	30.4752
	3	42.0090	44.8217	39.5410	42.4785	41.9408	41.7608	44.5524	39.2306	42.2260	41.6130
	4	62.8958	66.6348	54.5153	58.0802	58.4091	62.5705	66.2102	54.3911	58.1286	58.1962
	5	62.9299	67.9455	54.5968	58.6866	58.9230	62.8091	67.8541	54.5583	58.6572	58.8065
	6	63.2796	68.4193	60.1948	63.2074	63.7468	63.2579	68.3908	59.7620	62.7999	63.3072
0.28	1	30.1508	33.8769	26.3956	30.2290	30.2077	29.9396	33.6569	26.1365	30.0577	29.9209
	2	33.9292	37.0729	31.1257	34.0169	34.0726	33.8587	36.9977	31.0058	33.9754	33.9356
	3	45.1412	50.4032	41.4631	46.5425	45.3649	44.8892	50.0952	41.1629	46.3076	45.0311
	4	66.5749	74.4489	61.8068	66.6737	66.6156	66.2012	73.9391	61.3780	66.7576	66.3610
	5	70.1939	76.3330	62.1748	66.7656	67.2842	70.1088	76.2203	62.0728	66.8047	67.1422
	6	70.8833	76.8764	62.8157	67.3603	68.5631	70.8597	76.8395	62.7800	66.9449	68.1636

Table 4: Comparison of the frequency parameters Ω for a FG-CNT reinforced composite panel with SDSDSDSD boundary condition.

V^*_{tcn}	Mode	Ref [28]					Prsent Method				
		UD-CNT	FGX-CNT	FGO-CNT	FGV-CNT	FGΛ-CNT	UD-CNT	FGX-CNT	FGO-CNT	FGV-CNT	FGΛ-CNT
0.12	1	17.9355	19.8544	15.2680	16.5635	16.1755	17.8728	19.7953	15.1910	16.5152	16.0746
	2	20.7580	22.6972	18.3274	19.7483	19.2934	20.5977	22.5203	18.1042	19.5867	19.0512
	3	31.5916	33.5735	29.8442	31.1231	31.0416	31.4907	33.3135	29.5558	31.0173	30.7305
	4	34.1437	34.2505	34.2505	34.2496	34.2496	34.1467	34.2589	34.2587	34.2587	34.2269
	5	34.1448	34.2516	34.2516	34.2506	34.2508	34.1521	34.2591	34.2589	34.2906	34.2587
	6	48.3604	51.1737	41.6783	44.6667	44.7177	48.3344	50.8665	41.6455	44.6820	44.6331
0.17	1	22.3332	24.8189	19.0707	20.6504	20.2043	22.2492	24.7401	18.9671	20.5936	20.0560
	2	26.1225	28.7742	22.9868	24.9482	24.3929	25.8748	28.5387	22.6763	24.6887	24.0530
	3	40.5625	43.5052	37.8912	40.1570	39.9410	40.2295	43.1609	37.4804	39.7863	39.5087
	4	44.1116	44.4268	44.4268	44.4241	44.4241	44.1309	44.4460	44.4456	44.4454	44.3820
	5	44.1128	44.4280	44.4280	44.4257	44.4257	44.1309	44.4464	44.4460	44.5090	44.4454
	6	60.6570	65.7565	51.8039	55.6887	55.8671	60.6261	65.7253	51.7592	55.7326	55.7317
0.28	1	25.6520	28.8036	21.8402	23.6528	23.4884	25.5732	28.7221	21.7466	23.6266	23.3164
	2	29.2961	33.1701	25.1942	27.8317	27.6106	29.0560	32.9233	24.8948	27.5827	27.2580
	3	43.6590	47.4945	39.5216	43.3454	43.4505	43.3208	47.5075	39.1058	42.9546	43.0144
	4	46.2285	47.4962	47.4945	47.4848	47.4848	46.2424	47.5084	47.5067	47.5051	47.3676
	5	46.2302	49.1346	47.4962	47.4879	47.4879	46.2424	48.7519	47.5075	47.6433	47.5051
	6	66.8424	74.0069	59.9885	63.9651	64.3941	66.4770	73.9674	59.9562	64.0749	64.2075

Table 5: Comparison of the frequency parameters Ω for a FG-CNT reinforced composite panel with CFFF boundary condition.

V^*_{tcn}	Mode	Ref [28]					Prsent Method				
		UD-CNT	FGX-CNT	FGO-CNT	FGV-CNT	FGΛ-CNT	UD-CNT	FGX-CNT	FGO-CNT	FGV-CNT	FGΛ-CNT
0.12	1	6.3903	7.3335	5.1275	5.6401	5.6361	6.3891	7.3313	5.1270	5.6441	5.6278
	2	7.0793	7.9060	6.0180	6.3407	6.5225	7.1193	7.9406	6.0664	6.3928	6.5559
	3	10.0725	10.8363	9.2289	9.9216	9.4956	9.9337	10.6961	9.0807	9.7837	9.3393
	4	16.5033	16.5537	16.5510	16.5444	16.5363	16.5029	16.5534	16.5503	16.5627	16.5155
	5	20.0043	20.9329	19.2030	20.0002	19.8863	19.8084	20.7140	19.0088	19.7987	19.6778
	6	27.9595	30.5250	23.4902	25.4410	25.4711	27.9614	30.5207	23.4983	25.4497	25.4661
0.17	1	7.8415	9.0336	6.2882	6.9253	6.9199	7.8401	9.0305	6.2880	6.9297	6.9097
	2	8.7636	9.8005	7.4847	7.8772	8.0991	8.8180	9.8484	7.5488	7.9454	8.1464
	3	12.7766	13.8874	11.6685	12.6278	12.1425	12.5943	13.6958	11.4713	12.4461	11.9296
	4	21.2590	21.4059	21.4007	21.3910	21.3886	21.2615	21.4084	21.4025	21.4312	21.3533
	5	25.7353	27.4142	24.4613	25.8294	25.7404	25.4817	27.1152	24.1961	25.5518	25.4592
	6	34.8605	38.3864	28.9984	31.5500	31.5909	34.8658	38.3817	29.0102	31.5628	31.5866
0.28	1	9.3470	10.8558	7.4288	8.2577	8.2504	9.3459	10.8509	7.4307	8.2594	8.2444
	2	10.2233	11.5759	8.6491	9.2487	9.4009	10.2742	11.6213	8.7117	9.3093	9.4548
	3	14.0503	15.9281	12.4702	13.7821	13.5038	13.8690	15.7158	12.2794	13.6052	13.2787
	4	22.4329	23.0270	23.0232	23.0023	23.0198	22.4351	23.0286	23.0237	23.0839	22.9500
	5	27.2812	30.8404	25.0781	27.5845	27.6655	27.0181	30.4835	24.8161	27.2788	27.3792
	6	39.7825	43.8690	33.9831	36.7910	36.7957	39.7873	43.8550	34.0074	36.8053	36.8082

panels with general elastic supports. In this section, some results and discussions about the free vibration of moderately thick functionally graded carbon nanotube reinforced composite cylindrical panels are presented to verify the accuracy and flexibility of the proposed method. Firstly, the convergence, accuracy and reliability of the present method are presented by comparing with other contributions. Secondly, the vibration results of the moderately thick functionally graded carbon nanotube reinforced composite cylindrical panels with various boundary conditions including the classical, elastic and their combinations are presented. Then, the influence of elastic restrain parameters, thickness, subtended angle and volume fraction of carbon nanotubes on the free vibration characteristic of the cylindrical panels is also reported. In addition, in order to simplify this study, a symbolism is employed to represent the boundary condition of cylindrical panels, e.g. FCSE denotes the panels with F (Free), C (Clamped), S (simply-support) and E (Elastic restrain) boundary conditions at $x = 0$, $\theta = 0$, $x = L$ and $\theta = \phi$. Ta-

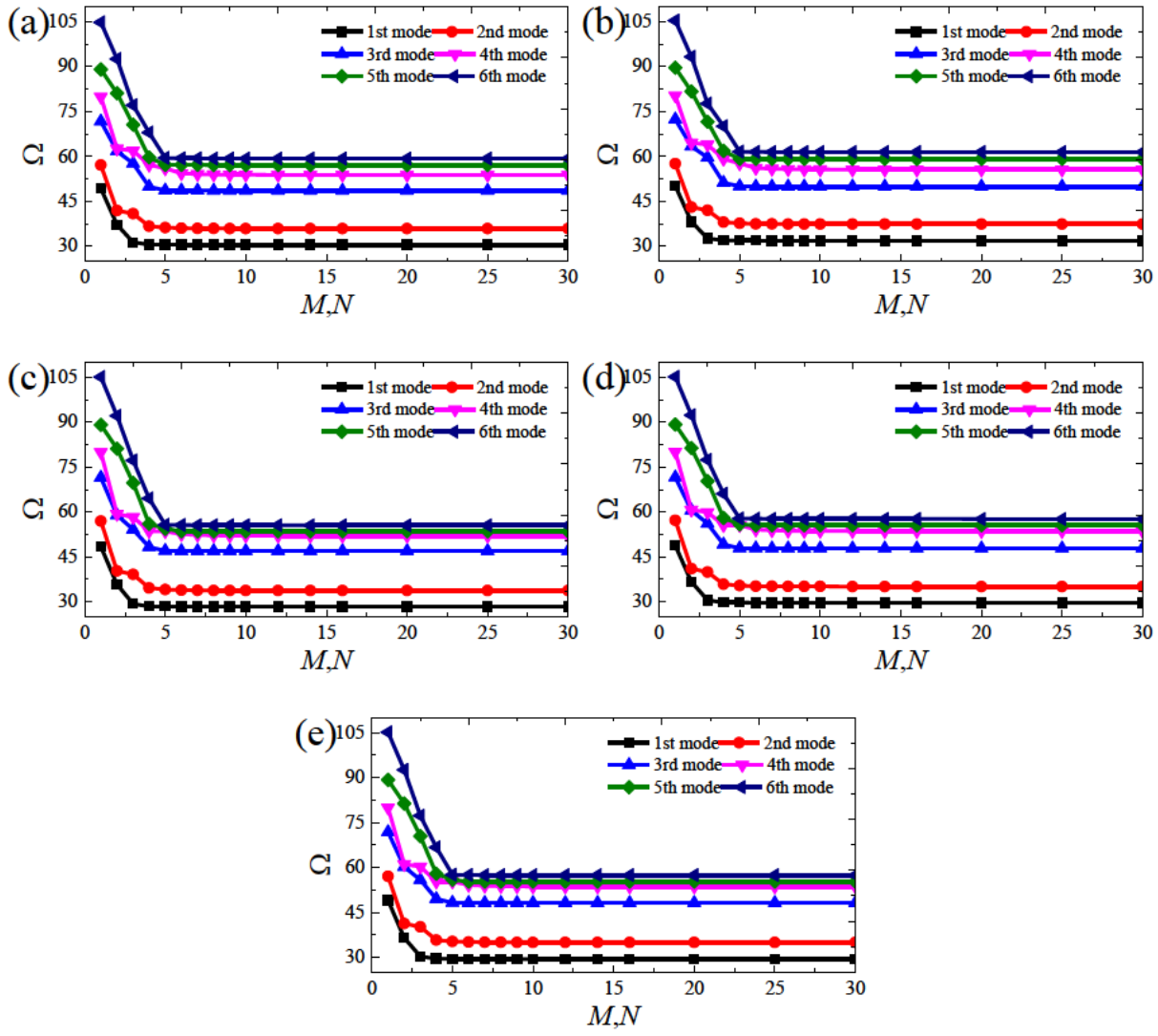

Figure 4: Convergence of frequency parameters Ω for a clamped FG-CNT reinforced composite panel with different distribution types: (a) UD-CNT; (b) FGX-CNT; (c) FGO-CNT; (d) FGV-CNT; (e) FGΛ-CNT.

ble 1 gives the corresponding spring stiffness values for the considered boundaries. Unless mentioned otherwise, the following material constants are used in this study: E^m = 2.5 GPa, μ^m = 0.34, ρ^m = 1150 kg/m^3, E_{11}^{cnt} = 5.6466 TPa, E_{22}^{cnt} = 7.0800 TPa, G_{12}^{cnt} = 1.9445 TPa, μ_{12}^{cnt} = 0.175 and ρ^{cnt} = 1150 kg/m^3. By matching with the results from molecular dynamics simulations, three types of the CNT efficiency parameters are given as: η_1 = 0.137, η_3 = 0.715, η_2 = 1.022 for V_{tcnt} = 0.12; η_1 = 0.142, η_3 = 1.626, η_2 = 1.138 for V_{tcnt} = 0.17; η_1 = 0.141, η_3 = 1.585, η_2 = 1.109 for V_{tcnt} = 0.28. Beyond that, the non-dimensional frequency parameter of the natural frequency are used in this study unless otherwise stated: $\Omega = \omega L^2/h\sqrt{\rho^m/E^m}$.

3.1 Convergence study and formulation validation

From the theoretical formulations, we can know that the computational accuracy relies on a limited number of terms in the displacement expressions in actual calculation. Thus, one important issue is the choice of the appropriate truncation terms. Figure 4 shows the convergence studies of the first six frequency parameters for a clamped FG-CNT reinforced composite panel with different distribution types and truncated numbers M, N. The geometrical dimensions of the panels are used: R = 1m, L = 2m, h = 0.1m, ϕ = 120°. From the figure, we can know that the proposed method has fast convergence and good stability. In view of the excellent numerical behavior of the current

Table 6: Fundamental frequency parameters Ω for FG-CNT reinforced composite panels with various boundary conditions and CNT volume fractions V_{tcnt}=0.12.

θ_0	Type	Boundary conditions							
		CCCC	SSSS	SDSDSD	CFCF	CE^1CE^1	$E^1E^1E^1E^1$	$E^2E^2E^2E^2$	$E^3E^3E^3E^3$
30°	UD-CNT	90.2446	59.1159	34.1521	24.6337	90.2432	90.2271	85.1135	85.0878
	FGX-CNT	92.4337	60.7731	34.2597	26.3480	92.4323	92.4161	87.2808	87.2551
	FGO-CNT	88.4674	57.8621	34.2581	21.2457	88.4658	88.4497	83.2322	83.2055
	FGV-CNT	90.1191	60.9068	34.3223	22.7933	90.1119	90.0919	84.9725	84.9274
	FGV1 -CNT	90.4886	57.7974	34.1951	22.8002	90.4886	90.4752	85.2319	85.2189
60°	UD-CNT	48.6159	42.3499	20.8355	24.9273	48.6147	48.5825	43.5090	43.4649
	FGX-CNT	49.9618	43.5005	22.5638	26.5845	49.9607	49.9283	44.8570	44.8134
	FGO-CNT	46.9337	41.3174	18.6107	21.7081	46.9324	46.8996	41.6205	41.5737
	FGV-CNT	47.8281	42.7483	20.1348	23.2067	47.8257	47.7892	42.6537	42.6001
	FGV1 -CNT	48.1237	41.9630	19.1466	23.1847	48.1229	48.0941	42.7972	42.7578
120°	UD-CNT	30.5208	23.2233	20.8355	25.2090	30.5207	30.4890	30.1008	30.0716
	FGX-CNT	31.8506	24.6307	22.5638	26.8086	31.8506	31.8185	31.4261	31.3969
	FGO-CNT	28.3578	21.5021	18.6107	22.1063	28.3577	28.3255	27.9236	27.8932
	FGV-CNT	29.6383	23.1328	20.1348	23.5058	29.6382	29.6026	29.1932	29.1601
	FGV1 -CNT	29.3685	22.9827	19.1466	23.5418	29.3685	29.3397	28.9587	28.9317

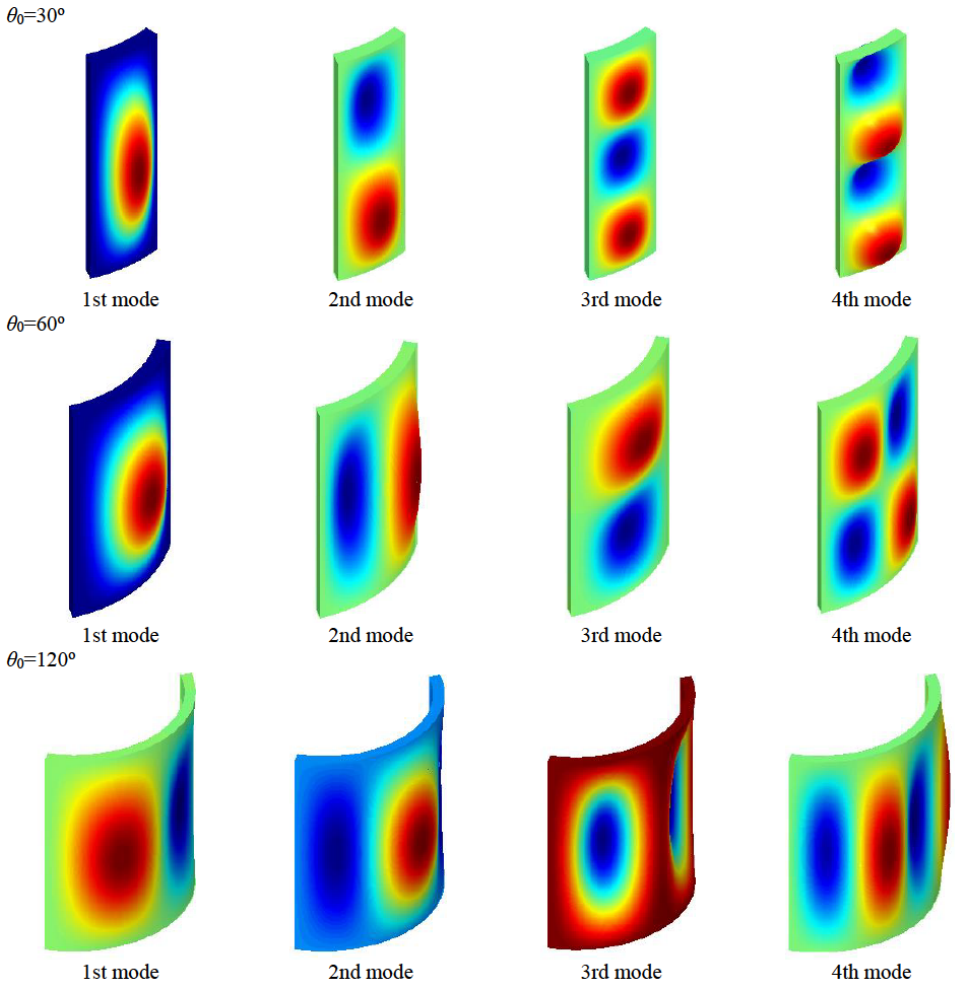

Figure 5: Mode shapes of the CCCC FG-CNT reinforced composite panel with UD-CNT type and volume fraction V_{tcnt}=0.12.

Table 7: Fundamental frequency parameters Ω for FG-CNT reinforced composite panels with various boundary conditions and CNT volume fractions $V_{tcnt} = 0.17$.

θ_0	Type	Boundary conditions							
		CCCC	SSSS	SDSDSD	CFCF	CE^1CE^1	$E^1E^1E^1E^1$	$E^2E^2E^2E^2$	$E^3E^3E^3E^3$
30°	UD-CNT	116.398	76.1524	44.1309	30.9204	116.396	116.371	108.043	107.989
	FGX-CNT	120.704	79.1941	44.4476	33.3878	120.702	120.677	112.267	112.212
	FGO-CNT	113.533	74.3004	44.4444	26.3480	113.530	113.505	104.939	104.882
	FGV-CNT	116.611	79.9430	44.5723	28.4205	116.599	116.566	108.148	108.056
	FGV1 -CNT	117.270	73.6745	44.3185	28.4316	117.270	117.250	108.684	108.654
60°	UD-CNT	62.3909	54.3582	26.2292	31.3509	62.3888	62.3399	53.1603	53.0639
	FGX-CNT	64.6761	56.0956	28.5865	33.7519	64.6741	64.6247	55.3776	55.2815
	FGO-CNT	60.1553	53.2495	23.4457	27.0044	60.1529	60.1025	50.4546	50.3495
	FGV-CNT	61.5220	55.3830	25.4238	29.0346	61.5179	61.4607	52.0747	51.9571
	FGV1 -CNT	61.9851	53.7194	24.2428	29.0045	61.9837	61.9404	52.2716	52.1819
120°	UD-CNT	38.8851	29.4694	26.2292	31.7283	38.8850	38.8363	38.0639	38.0197
	FGX-CNT	40.9757	31.4155	28.5865	34.0413	40.9756	40.9257	40.1372	40.0930
	FGO-CNT	35.9446	27.3668	23.4457	27.5607	35.9445	35.8941	35.0827	35.0347
	FGV-CNT	37.7596	29.4518	25.4238	29.4393	37.7594	37.7034	36.8831	36.8310
	FGV1 -CNT	37.4692	29.2670	24.2428	29.4886	37.4692	37.4246	36.6551	36.6135

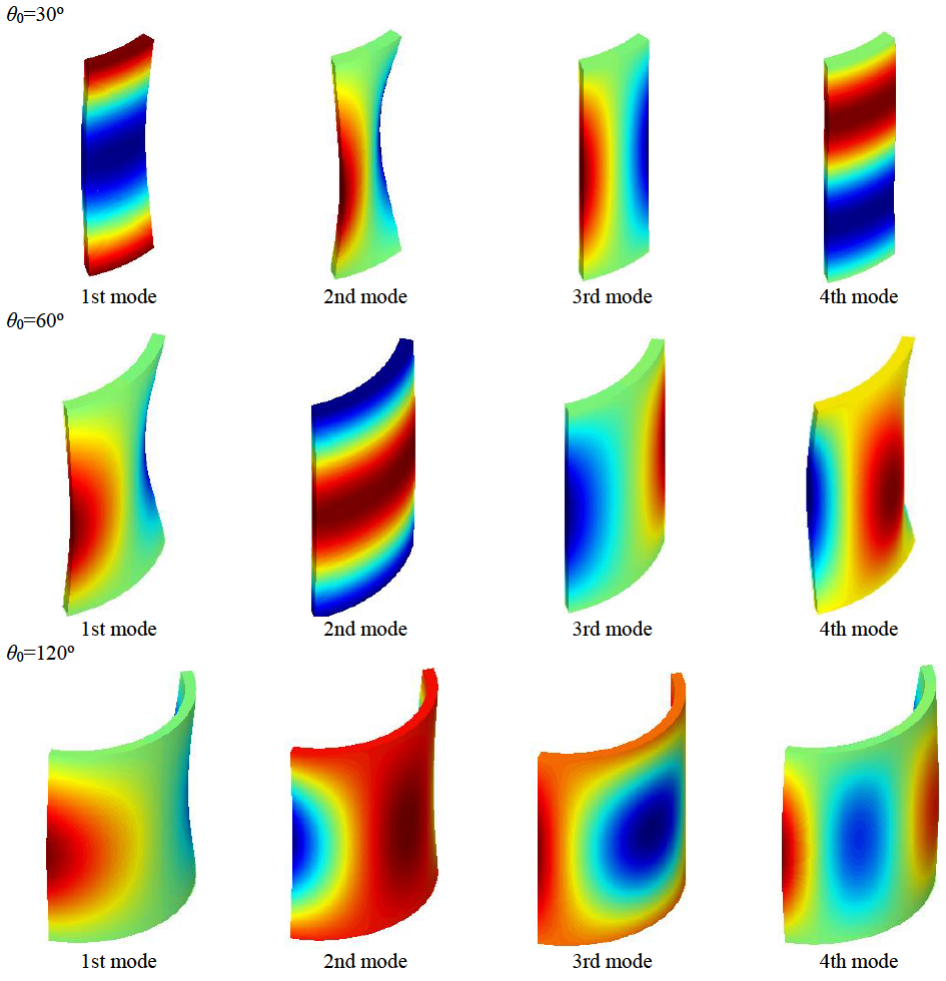

Figure 6: Mode shapes of the CFCF FG-CNT reinforced composite panel with FGX-CNT type and volume fraction V_{tcnt}=0.17.

Table 8: Fundamental frequency parameters Ω for FG-CNTRC panels with various boundary conditions and CNT volume fractions V_{tcnt} = 0.28.

θ_0	Type	Boundary conditions							
		CCCC	SSSS	SDSDSD	CFCF	CE^1CE^1	$E^1E^1E^1E^1$	$E^2E^2E^2E^2$	$E^3E^3E^3E^3$
30°	UD-CNT	122.450	80.3386	46.2424	34.6755	122.449	122.431	113.358	113.306
	FGX-CNT	132.251	87.0760	47.5112	37.4418	132.249	132.231	122.786	122.729
	FGO-CNT	118.311	77.6772	47.5043	30.6869	118.310	118.290	108.599	108.540
	FGV-CNT	124.422	89.2772	47.7806	32.7608	124.416	124.389	114.744	114.658
	FGV1 -CNT	125.631	75.5997	47.2295	32.7633	125.631	125.617	116.168	116.132
60°	UD-CNT	66.4262	57.9115	29.3136	35.0037	66.4250	66.3904	56.2645	56.1760
	FGX-CNT	70.6525	61.2037	32.7186	37.7808	70.6513	70.6153	59.9573	59.8621
	FGO-CNT	64.5143	55.3999	25.8432	31.1574	64.5128	64.4756	53.4350	53.3307
	FGV-CNT	66.5873	60.0471	28.1820	33.2586	66.5850	66.5429	55.6853	55.5726
	FGV1 -CNT	67.1998	56.9252	27.5399	33.2239	67.1989	67.1672	56.1845	56.0931
120°	UD-CNT	42.1198	32.3099	29.3136	35.3653	42.1198	42.0832	41.1760	41.1438
	FGX-CNT	45.3062	35.3100	32.7186	38.0413	45.3062	45.2663	44.2805	44.2463
	FGO-CNT	39.3355	29.8131	25.8432	31.7433	39.3355	39.2954	38.3182	38.2807
	FGV-CNT	41.4683	32.6392	28.1820	33.6910	41.4682	41.4242	40.4395	40.3994
	FGV1 -CNT	41.5438	32.5238	27.5399	33.6832	41.5438	41.5077	40.5630	40.5304

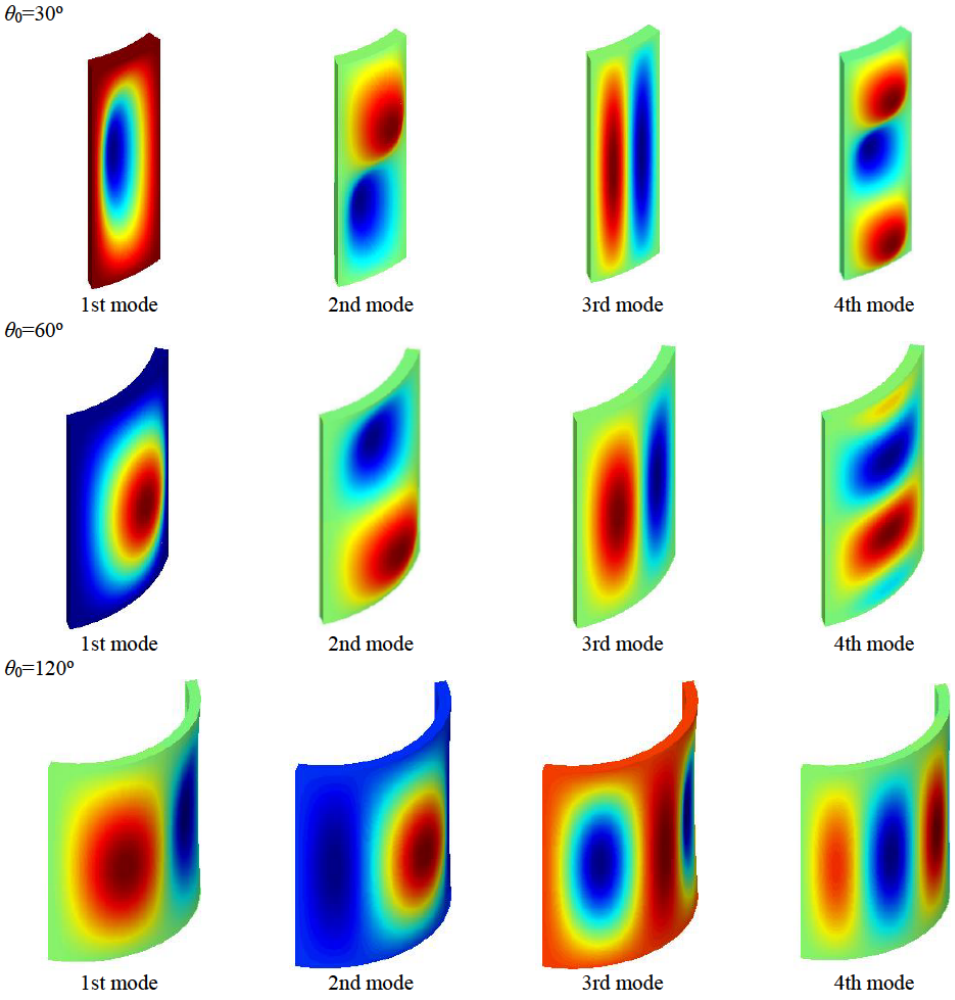

Figure 7: Mode shapes of the $E^3E^3E^3E^3$ FG-CNT reinforced composite panel with FGV-CNT type and volume fraction V_{tcnt}=0.28.

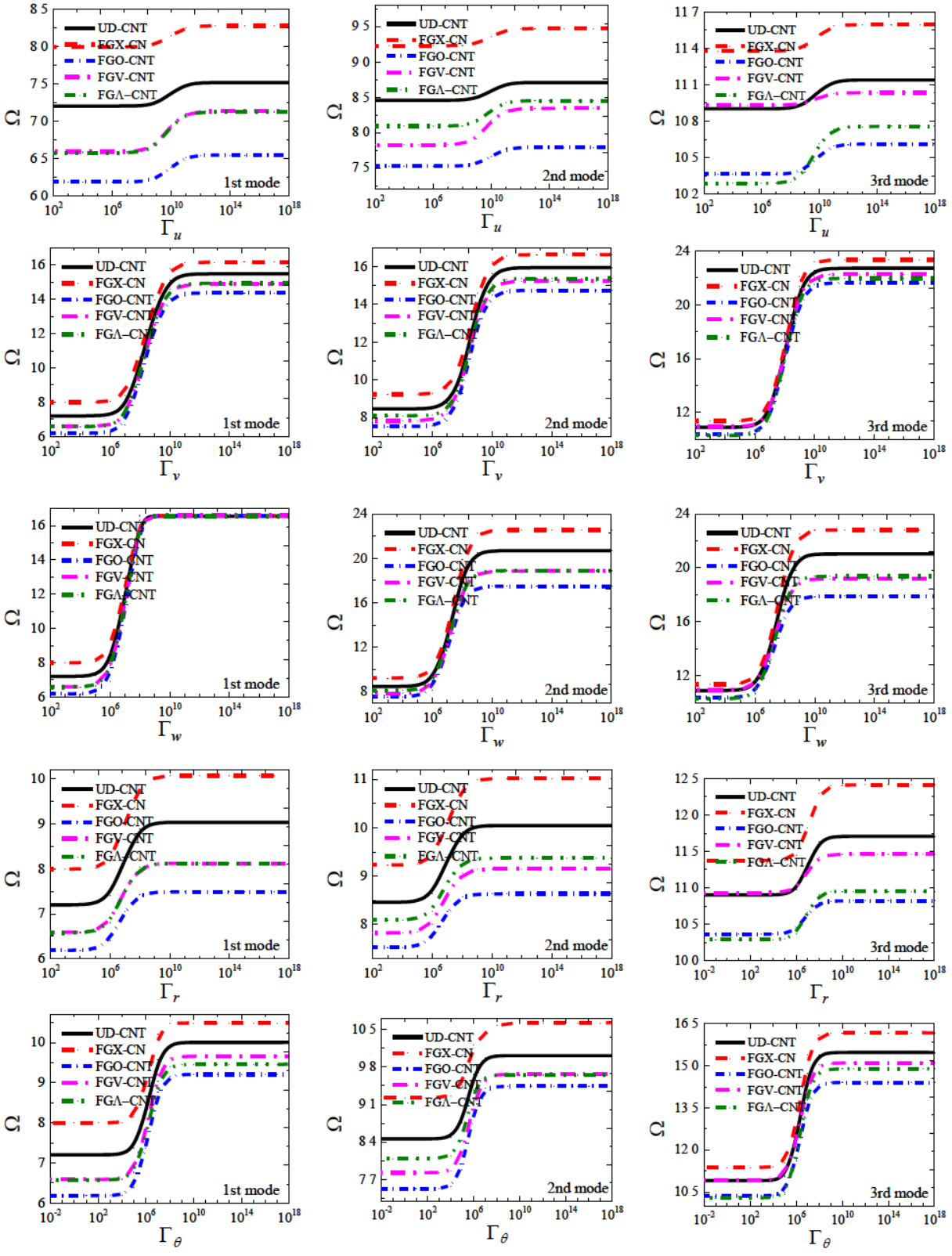

Figure 8: Variation of the first three frequency parameters Ω versus the elastic restraint parameters for FG-CNT reinforced composite panel with CCCC boundary condition (V_{tcnt}=0.12).

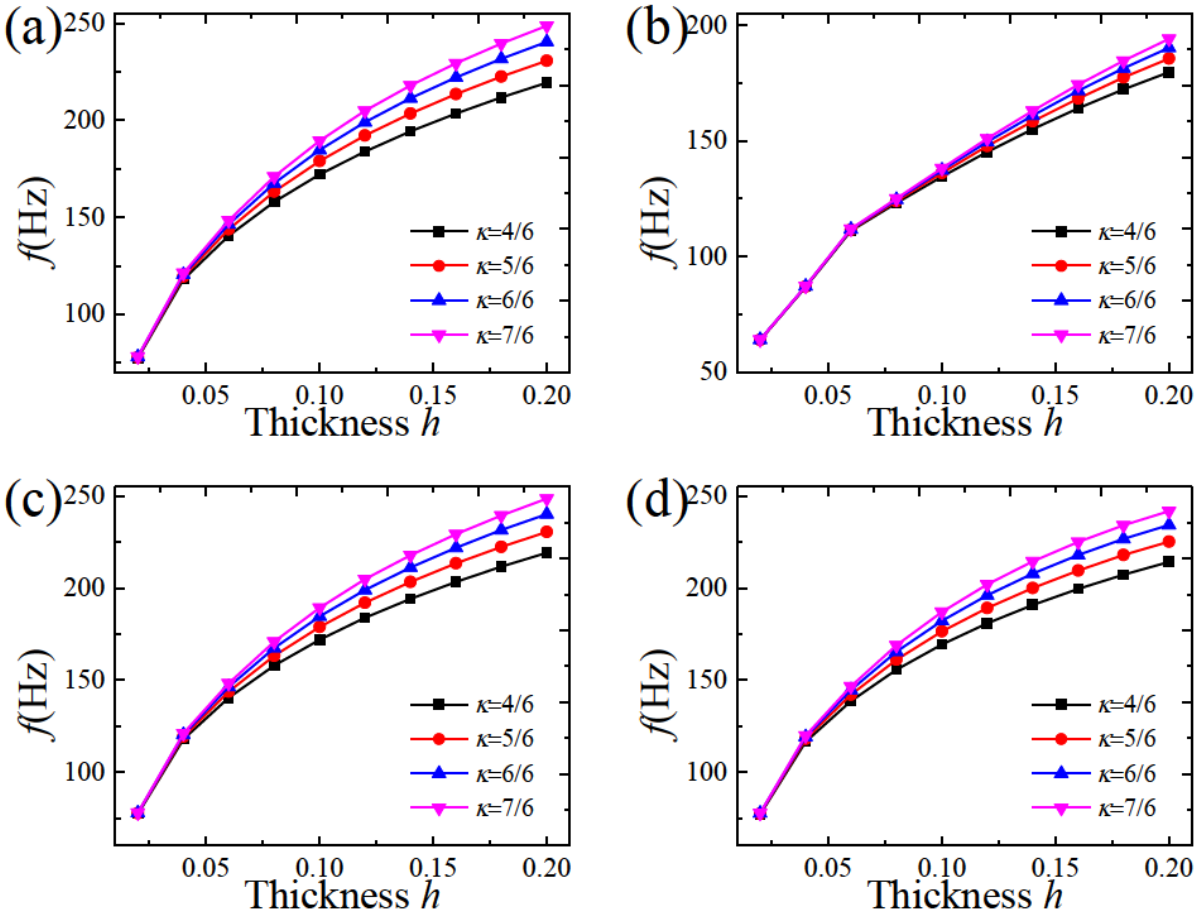

Figure 9: Fundamental frequency parameters versus thickness h for the UD-CNT panel with different shear correction factors and boundary conditions (V_{tcnt}=0.12): (a) CCCC; (b) SSSS; (c) $E^1E^1E^1E^1$; (d) $E^3E^3E^3E^3$.

solution, the truncation numbers will be simply set as $M = N = 15$ in the following calculations.

The corresponding studies are performed by comparing the present results with the existing published results to validate the present method used in this study. The validation results for the different boundary conditions are shown in Tables 2–5. The geometrical parameters for the panels are given as follows: $L = 1$, $R = 1$, $h = 0.05$, $\phi = 1$. In order to check the present method, the numerical results reported by Mirzaei and Kiani [28] using the Ritz method on the basis of FSDT are also given in the above tables for comparison. From the comparisons, we can see a consistent agreement of the results taken from the current method and referential data. Besides, Tables 2–5 also show that it is appropriate to define the classical boundary conditions in terms of the boundary spring rigidities as shown in Table 1.

Based on the validation studies, some new results for the FG-CNT reinforced composite panel with classical-elastic and elastic restraint boundary conditions are shown in Tables 6–8. Also, for any given modal frequency, the corresponding mode shape can be easily determined by submitting the solved eigenvector into Eq. (19). Thus, some selected mode shapes are performed in the Figures 5–7.

3.2 Parameter studies

Although the above results of the FG-CNT reinforced composite cylindrical panel with classical-elastic and elastic restraint boundary conditions can be served as benchmark data for the future numerical methods, it does not meet authors' ambition. The goal of this paper is to present a unified solution of the free vibration for the FG-CNT reinforced composite cylindrical panels to provide some useful research works for the designer or engineer to avoid the unpleasant, inefficient and structurally damaging resonant. So, in the this subsection, the parameter studies including the elastic restraint parameters, thickness, sub-

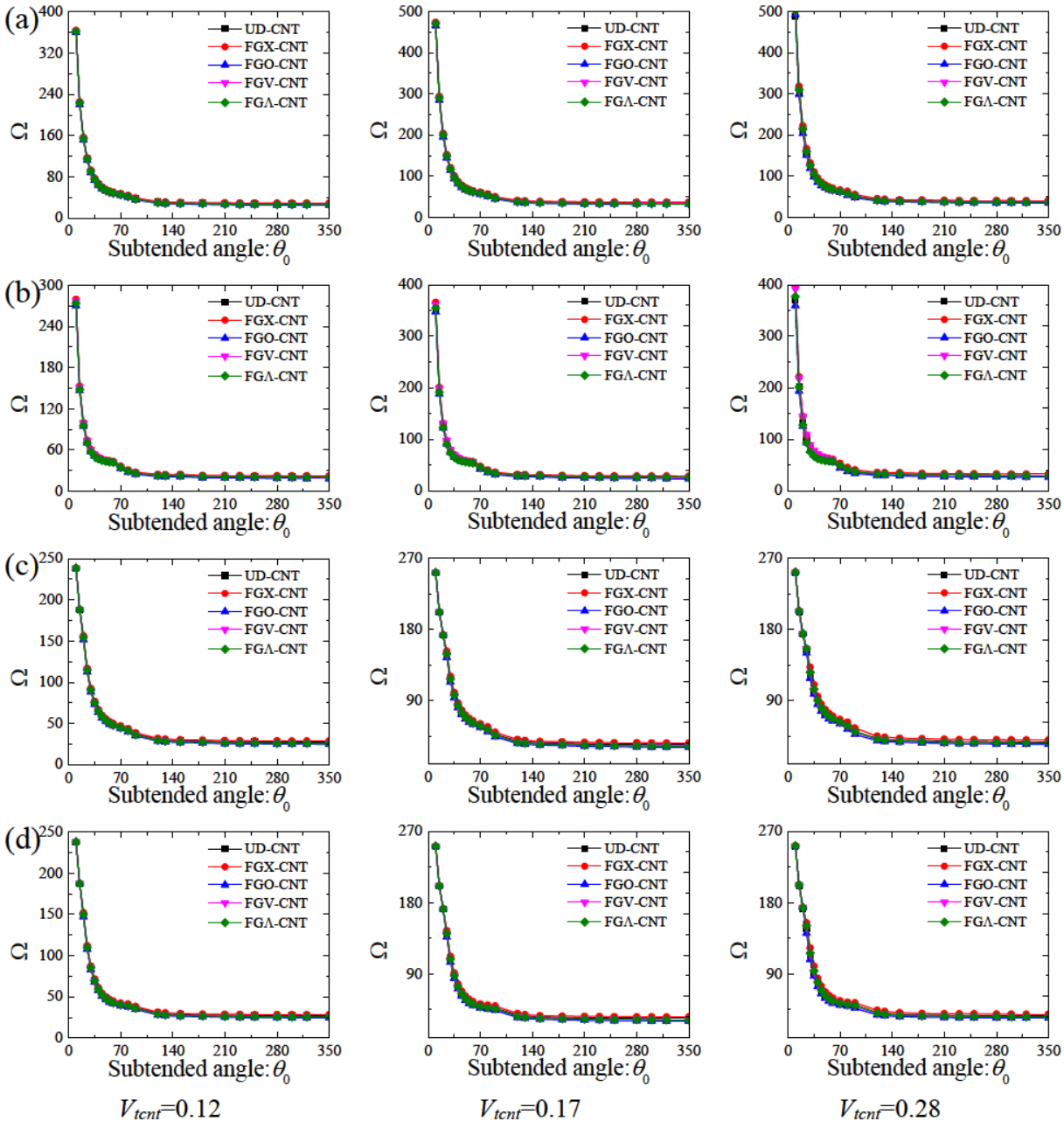

Figure 10: Variation of the fundamental frequency parameters Ω versus the subtended angle for FG-CNT reinforced composite panel with various boundary conditions: (a) CCCC; (b) SSSS; (c) $E^1E^1E^1E^1$; (d) $E^3E^3E^3E^3$.

tended angle and volume fraction of carbon nanotubes are presented.

Figure 8 shows the effects of all kinds of boundary restraint parameters on the frequecny paramerters of FG-CNT reinforced composite cylindrical panels with elastic boundary conditions. The geometry properties of the panels studied are the same as those in Figure 4. The panles are free at edges θ = constant, clamped at x = 0 whilst at $x = L$ they are elastically restrained by all the five groups of boundary springs, of which only one group is with the variable stiffness and the others are assumed to be zeros. From Figure 8, it is observed that the frequency parameters increase rapidly as the restraint parameters increase in the certain range. And beyond this range, there is little variations in the frequencies. In addition, we can know that the FGX-CNT panels always have the higher frequency parameters and the FGO-CNT panels have the minimum frequency parameters. Figure 9 depictes the fundamental

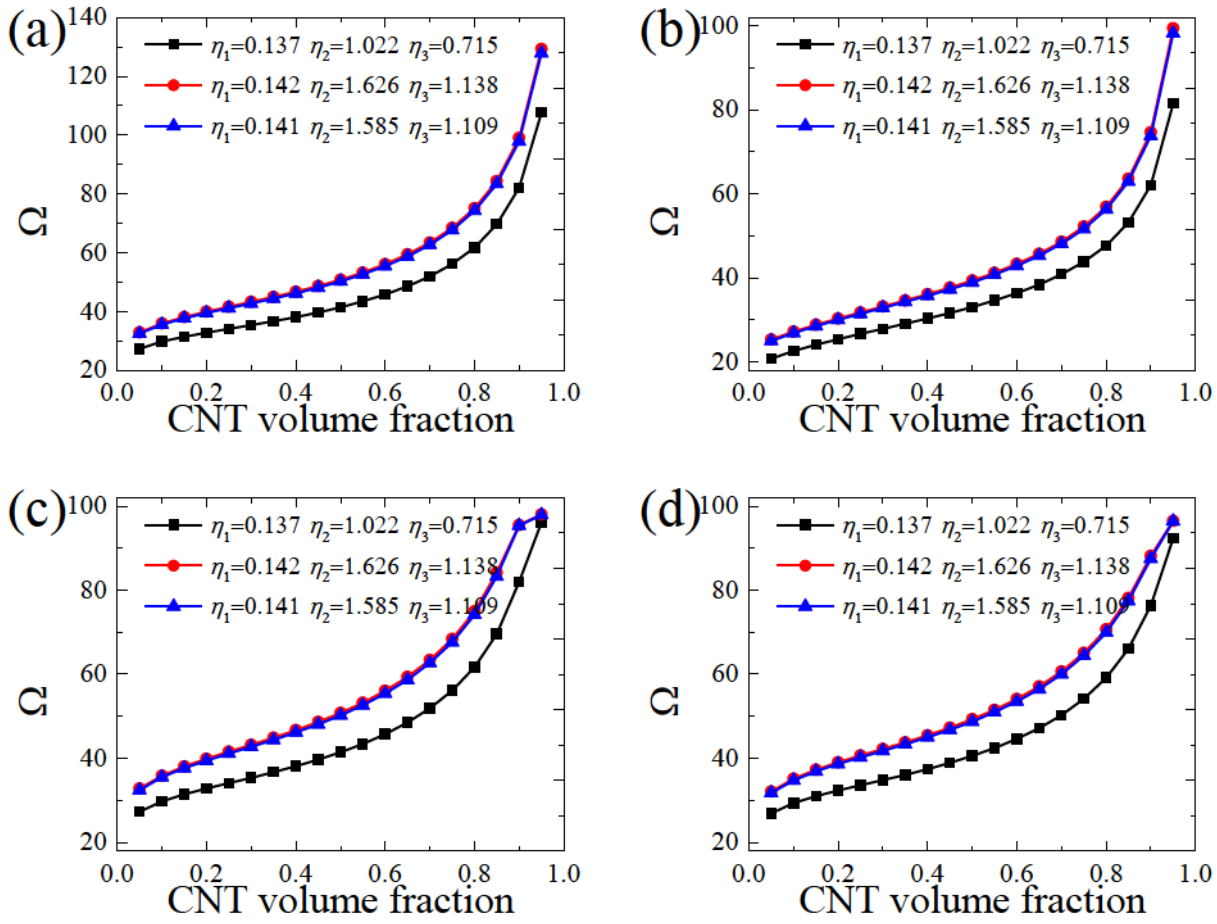

Figure 11: Variation of the fundamental frequency parameters Ω versus the CNT volume fraction V_{tcnt} for FG-CNT reinforced composite panel with various boundary conditions: (a) CCCC; (b) SSSS; (c) $E^1E^1E^1E^1$; (d) $E^3E^3E^3E^3$.

frequency parameters versus thickness h for the UD-CNT panel with different shear correction factors and boundary conditions (CCCC, SSSS, $E^1E^1E^1E^1$, $E^3E^3E^3E^3$). It is seen from the numerical results that, in all of the cases, increasing the thickness of CNT results in higher natural frequencies. In addition, the figures also show that the effect of the shear correction factor κ increases generally as the thickness h increases. Furthermore, a larger shear correction factor will result in higher frequency parameters. Next, Figure 10 presents the fundamental frequency parameters for the FG-CNT reinforced composite panel versus the subtended angle with the CCCC, SSSS, $E^1E^1E^1E^1$, $E^3E^3E^3E^3$ boundary conditions and different functionally graded CNT cylindrical panel types. From the figure, we can see that, regardless of the boundary condition and FG-CNT type, the frequency parameters rapidly decrease while the subtended angle is changed from 5° to 100°, and out of this range the frequency parameters slowly minish and lastly almost remain unchanged. Figure 11 shows the influence of the volume fraction of carbon nanotubes on the vibration behavior of the FG-CNT reinforced composite cylindrical panel with different boundary conditions and efficiency parameters. It is observed that the frequency parameters increase while increasing the volume fraction of carbon nanotubes regardless of the type of the boundary conditions and efficiency parameters.

4 Conclusions

In this paper, a unified solution is presented for the vibration analysis of the FG-CNT cylindrical panel with general elastic supports based on the first-order shear deformation theory. A enhanced Ritz method is presented based on the Ritz-variational energy method in conjunction with the modified Fourier series method. Distribution of CNT across the panel thickness may be uniform or functionally graded. Properties of the composite media are obtained according to a refined rule of mixtures

approach with the introduction of efficiency parameters into the rule of mixtures approach. Five types of aligned CNT reinforced cylindrical panels are considered: namely the uniformly distributed CNT cylindrical panel(UD-CNT), functionally graded CNT cylindrical panel type V(FGV-CNT), functionally graded CNT cylindrical panel type Λ(FGΛ-CNT), functionally graded CNT cylindrical panel type X(FGX-CNT), and functionally graded CNT cylindrical panel type O(FGO-CNT). The good convergence, excellent accuracy and reliability of the present unified solution are checked and validated by the comparison with the results presented by other contributors. New results for free vibration of moderately thick FG-CNT cylindrical panel with various geometric parameters, material parameters as well as the boundary conditions are presented, which may be used for benchmarking of researchers in the field. Also, the influence of elastic restraint parameters, thickness, subtended angle and volume fraction of carbon nanotubes on the free vibration characteristic of the cylindrical panels are also reported. The following conclusions can be drawn as:

1. The frequency parameters increase rapidly as the restraint parameters increase in the certain range. And beyond this range, there is little variations in the frequencies.item Regardless of the boundary condition, increasing the thickness of CNT results in higher natural frequencies. In addition, the effects of the shear correction factor κ increase generally as the thickness h increases. Furthermore, a larger shear correction factor will result in higher frequency parameters.
2. Regardless of the boundary condition and FG-CNT type, the frequency parameters of the FG-CNT cylindrical panel rapidly decrease while the subtended angle is changed from 5° to 100°, and out of this range the frequency parameters slowly minish and lastly almost remain unchanged.
3. The frequency parameters of the FG-CNT cylindrical panel increase while increasing the volume fraction of carbon nanotubes regardless of the type of the boundary conditions and efficiency parameters. In addition, the FGX-CNT panels always have the higher frequency parameters and the FGO-CNT panels have the minimum frequency parameters.

Acknowledgement: The authors gratefully acknowledge the support of the National Natural Science Foundation of China (No. 51705537, 51535012, U1604255) and the Key research and development project of Hunan province (No. 2016JC2001).

References

[1] K. Liew, Z. Lei, L. Zhang, Mechanical analysis of functionally graded carbon nanotube reinforced composites: a review, Composite Structures, 120 (2015) 90-97.

[2] F. Lin, Y. Xiang, Vibration of carbon nanotube reinforced composite beams based on the first and third order beam theories, Appl. Math. Model., 38 (2014) 3741-3754.

[3] M. Rafiee, J. Yang, S. Kitipornchai, Large amplitude vibration of carbon nanotube reinforced functionally graded composite beams with piezoelectric layers, Composite Structures, 96 (2013) 716-725.

[4] L.-L. Ke, J. Yang, S. Kitipornchai, Nonlinear free vibration of functionally graded carbon nanotube-reinforced composite beams, Composite Structures, 92 (2010) 676-683.

[5] L.-L. Ke, J. Yang, S. Kitipornchai, M.A. Bradford, Bending, buckling and vibration of size-dependent functionally graded annular microplates, Composite structures, 94 (2012) 3250-3257.

[6] H.-S. Shen, Nonlinear bending of functionally graded carbon nanotube-reinforced composite plates in thermal environments, Composite Structures, 91 (2009) 9-19.

[7] P. Zhu, Z. Lei, K.M. Liew, Static and free vibration analyses of carbon nanotube-reinforced composite plates using finite element method with first order shear deformation plate theory, Composite Structures, 94 (2012) 1450-1460.

[8] L. Zhang, Z. Lei, K. Liew, Vibration characteristic of moderately thick functionally graded carbon nanotube reinforced composite skew plates, Composite Structures, 122 (2015) 172-183.

[9] L. Zhang, Z. Lei, K. Liew, Free vibration analysis of functionally graded carbon nanotube-reinforced composite triangular plates using the FSDT and element-free IMLS-Ritz method, Composite Structures, 120 (2015) 189-199.

[10] L. Zhang, Z. Lei, K. Liew, J. Yu, Static and dynamic of carbon nanotube reinforced functionally graded cylindrical panels, Composite Structures, 111 (2014) 205-212.

[11] P. Malekzadeh, A. Zarei, Free vibration of quadrilateral laminated plates with carbon nanotube reinforced composite layers, Thin-Walled Structures, 82 (2014) 221-232.

[12] P. Malekzadeh, Y. Heydarpour, Mixed Navier-layerwise differential quadrature three-dimensional static and free vibration analysis of functionally graded carbon nanotube reinforced composite laminated plates, Meccanica, 50 (2015) 143-167.

[13] S. Natarajan, M. Haboussi, G. Manickam, Application of higher-order structural theory to bending and free vibration analysis of sandwich plates with CNT reinforced composite facesheets, Composite Structures, 113 (2014) 197-207.

[14] Z.-X. Wang, H.-S. Shen, Nonlinear vibration of nanotube-reinforced composite plates in thermal environments, Computational Materials Science, 50 (2011) 2319-2330.

[15] Z.-X. Wang, H.-S. Shen, Nonlinear vibration and bending of sandwich plates with nanotube-reinforced composite face sheets, Composites Part B: Engineering, 43 (2012) 411-421.

[16] Z.-X. Wang, H.-S. Shen, Nonlinear dynamic response of nanotube-reinforced composite plates resting on elastic foundations in thermal environments, Nonlinear Dynamics, 70 (2012) 735-754.

[17] Z. Lei, L. Zhang, K. Liew, Elastodynamic analysis of carbon nanotube-reinforced functionally graded plates, International Journal of Mechanical Sciences, 99 (2015) 208-217.

[18] L. Zhang, Z. Song, K. Liew, State-space Levy method for vibration analysis of FG-CNT composite plates subjected to in-plane loads based on higher-order shear deformation theory, Composite Structures, 134 (2015) 989-1003.
[19] L. Zhang, W. Cui, K. Liew, Vibration analysis of functionally graded carbon nanotube reinforced composite thick plates with elastically restrained edges, International Journal of Mechanical Sciences, 103 (2015) 9-21.
[20] Z. Lei, L. Zhang, K. Liew, Free vibration analysis of laminated FG-CNT reinforced composite rectangular plates using the kp-Ritz method, Composite Structures, 127 (2015) 245-259.
[21] L. Zhang, Z. Lei, K. Liew, Buckling analysis of FG-CNT reinforced composite thick skew plates using an element-free approach, Composites Part B: Engineering, 75 (2015) 36-46.
[22] L. Zhang, K. Liew, J. Reddy, Postbuckling of carbon nanotube reinforced functionally graded plates with edges elastically restrained against translation and rotation under axial compression, Computer Methods in Applied Mechanics and Engineering, 298 (2016) 1-28.
[23] Z. Lei, L. Zhang, K. Liew, Analysis of laminated CNT reinforced functionally graded plates using the element-free kp-Ritz method, Composites Part B: Engineering, 84 (2016) 211-221.
[24] L. Zhang, K. Liew, Large deflection analysis of FG-CNT reinforced composite skew plates resting on Pasternak foundations using an element-free approach, Composite Structures, 132 (2015) 974-983.
[25] L. Zhang, Z. Song, K. Liew, Nonlinear bending analysis of FG-CNT reinforced composite thick plates resting on Pasternak foundations using the element-free IMLS-Ritz method, Composite Structures, 128 (2015) 165-175.
[26] L. Zhang, K. Liew, Geometrically nonlinear large deformation analysis of functionally graded carbon nanotube reinforced composite straight-sided quadrilateral plates, Computer Methods in Applied Mechanics and Engineering, 295 (2015) 219-239.
[27] Z. Lei, L. Zhang, K. Liew, J. Yu, Dynamic stability analysis of carbon nanotube-reinforced functionally graded cylindrical panels using the element-free kp-Ritz method, Composite Structures, 113 (2014) 328-338.
[28] M. Mirzaei, Y. Kiani, Free Vibration of Functionally Graded Carbon Nanotube Reinforced Composite Cylindrical Panels, Composite Structures, (2016).
[29] F. Tornabene, N. Fantuzzi, M. Bacciocchi, E. Viola, J.N. Reddy, A numerical investigation on the natural frequencies of FGM sandwich shells with variable thickness by the local generalized differential quadrature method, Applied Sciences, 7 (2017) 131.
[30] F. Tornabene, N. Francesco, E. Viola, Inter-laminar stress recovery procedure for doubly-curved, singly-curved, revolution shells with variable radii of curvature and plates using generalized higher-order theories and the local GDQ method, Mechanics of Advanced Materials and Structures, 23 (2016) 1019-1045.
[31] F. Tornabene, N. Fantuzzi, M. Bacciocchi, E. Viola, Effect of agglomeration on the natural frequencies of functionally graded carbon nanotube-reinforced laminated composite doubly-curved shells, Compos Part B-Eng, 89 (2016) 187-218.
[32] F. Tornabene, N. Fantuzzi, M. Bacciocchi, E. Viola, J. Reddy, A Numerical Investigation on the Natural Frequencies of FGM Sandwich Shells with Variable Thickness by the Local Generalized Differential Quadrature Method, Applied Sciences, 7 (2017) 131.
[33] F. Tornabene, N. Fantuzzi, M. Bacciocchi, J. Reddy, An Equivalent Layer-Wise Approach for the Free Vibration Analysis of Thick and Thin Laminated and Sandwich Shells, Applied Sciences, 7 (2017) 17.
[34] F. Tornabene, N. Fantuzzi, M. Bacciocchi, A new doubly-curved shell element for the free vibrations of arbitrarily shaped laminated structures based on Weak Formulation IsoGeometric Analysis, Composite Structures, 171 (2017) 429-461.
[35] S. Brischetto, F. Tornabene, N. Fantuzzi, M. Bacciocchi, Interpretation of boundary conditions in the analytical and numerical shell solutions for mode analysis of multilayered structures, International Journal of Mechanical Sciences, 122 (2017) 18-28.
[36] D. Banić, M. Bacciocchi, F. Tornabene, A. Ferreira, Influence of Winkler-Pasternak Foundation on the Vibrational Behavior of Plates and Shells Reinforced by Agglomerated Carbon Nanotubes, Applied Sciences, 7 (2017) 1228.
[37] F. Tornabene, S. Brischetto, N. Fantuzzi, M. Bacciocchi, Boundary Conditions in 2D Numerical and 3D Exact Models for Cylindrical Bending Analysis of Functionally Graded Structures, Shock Vibrat., 2016 (2016) 17.
[38] F. Tornabene, N. Fantuzzi, M. Bacciocchi, R. Dimitri, Free vibrations of composite oval and elliptic cylinders by the generalized differential quadrature method, Thin-Walled Struct., 97 (2015) 114-129.
[39] M.S. Qatu, Vibration of laminated shells and plates, Elsevier, 2004.
[40] G. Jin, X. Ma, S. Shi, T. Ye, Z. Liu, A modified Fourier series solution for vibration analysis of truncated conical shells with general boundary conditions, Applied Acoustics, 85 (2014) 82-96.
[41] T. Ye, G. Jin, Z. Su, Y. Chen, A modified Fourier solution for vibration analysis of moderately thick laminated plates with general boundary restraints and internal line supports, International Journal of Mechanical Sciences, 80 (2014) 29-46.
[42] W.L. Li, Free vibrations of beams with general boundary conditions, J. Sound Vibrat., 237 (2000) 709-725.
[43] Q. Wang, D. Shi, Q. Liang, X. Shi, A unified solution for vibration analysis of functionally graded circular, annular and sector plates with general boundary conditions, Composites Part B: Engineering, 88 (2016) 264-294.
[44] H. Zhang, D. Shi, S. Zha, Q. Wang, Vibro-acoustic analysis of the thin laminated rectangular plate-cavity coupling system, Composite Structures, 189 (2018) 570-585.
[45] Q. Wang, D. Shao, B. Qin, A simple first-order shear deformation shell theory for vibration analysis of composite laminated open cylindrical shells with general boundary conditions, Composite Structures, 184 (2018) 211-232.
[46] Q. Wang, K. Choe, D. Shi, K. Sin, Vibration analysis of the coupled doubly-curved revolution shell structures by using Jacobi-Ritz method, International Journal of Mechanical Sciences, 135 (2018) 517-531.
[47] J. Guo, D. Shi, Q. Wang, J. Tang, C. Shuai, Dynamic analysis of laminated doubly-curved shells with general boundary conditions by means of a domain decomposition method, International Journal of Mechanical Sciences, 138-139 (2018) 159-186.
[48] J. Guo, D. Shi, Q. Wang, F. Pang, Q. Liang, A domain decomposition approach for static and dynamic analysis of composite laminated curved beam with general elastic restrains, Mechanics of Advanced Materials and Structures, (2018) 1-13.
[49] X. Guan, J. Tang, Q. Wang, C. shuai, Application of the differential quadrature finite element method to free vibration of elastically restrained plate with irregular geometries, Engineering Analysis with Boundary Elements, 90 (2018) 1-16.

[50] Y. Zhou, Q. Wang, D. Shi, Q. Liang, Z. Zhang, Exact solutions for the free in-plane vibrations of rectangular plates with arbitrary boundary conditions, International Journal of Mechanical Sciences, 130 (2017) 1-10.

[51] H. Zhang, D. Shi, Q. Wang, B. Qin, Free vibration of functionally graded parabolic and circular panels with general boundary conditions, Curved and Layered Structures, 4 (2017) 52-84.

[52] H. Zhang, D. Shi, Q. Wang, An improved Fourier series solution for free vibration analysis of the moderately thick laminated composite rectangular plate with non-uniform boundary conditions, International Journal of Mechanical Sciences, 121 (2017) 1-20.

[53] Q. Wang, D. Shi, Q. Liang, F. Pang, Free vibration of four-parameter functionally graded moderately thick doubly-curved panels and shells of revolution with general boundary conditions, Appl. Math. Model., 42 (2017) 705-734.

[54] Q. Wang, D. Shi, Q. Liang, F. Pang, Free vibrations of composite laminated doubly-curved shells and panels of revolution with general elastic restraints, Appl. Math. Model., 46 (2017) 227-262.

[55] Q. Wang, D. Shi, Q. Liang, F. Pang, A unified solution for vibration analysis of moderately thick functionally graded rectangular plates with general boundary restraints and internal line supports, Mechanics of Advanced Materials and Structures, 24 (2017) 943-961.

[56] Q. Wang, B. Qin, D. Shi, Q. Liang, A semi-analytical method for vibration analysis of functionally graded carbon nanotube reinforced composite doubly-curved panels and shells of revolution, Composite Structures, 174 (2017) 87-109.

[57] Q. Wang, F. Pang, B. Qin, Q. Liang, A unified formulation for free vibration of functionally graded carbon nanotube reinforced composite spherical panels and shells of revolution with general elastic restraints by means of the Rayleigh–Ritz method, Polymer Composites, (2017) n/a-n/a.

[58] Q. Wang, X. Cui, B. Qin, Q. Liang, J. Tang, A semi-analytical method for vibration analysis of functionally graded (FG) sandwich doubly-curved panels and shells of revolution, International Journal of Mechanical Sciences, 134 (2017) 479-499.

[59] Q. Wang, X. Cui, B. Qin, Q. Liang, Vibration analysis of the functionally graded carbon nanotube reinforced composite shallow shells with arbitrary boundary conditions, Composite Structures, 182 (2017) 364-379.

[60] Q. Wang, D. Shi, F. Pang, Q. Liang, Vibrations of Composite Laminated Circular Panels and Shells of Revolution with General Elastic Boundary Conditions via Fourier-Ritz Method, Curved and Layered Structures, 3 (2016) 105-136.

Appendix. Detailed expressions of the matrices M, K and H

$$\mathbf{K}=\begin{bmatrix}\mathbf{K}_{uu} & \mathbf{K}_{uv} & \mathbf{K}_{uw} & \mathbf{K}_{ux} & \mathbf{K}_{u\theta}\\ \mathbf{K}_{uv}^T & \mathbf{K}_{vv} & \mathbf{K}_{vw} & \mathbf{K}_{vx} & \mathbf{K}_{v\theta}\\ \mathbf{K}_{uw}^T & \mathbf{K}_{vw}^T & \mathbf{K}_{ww} & \mathbf{K}_{wx} & \mathbf{K}_{w\theta}\\ \mathbf{K}_{ux}^T & \mathbf{K}_{vx}^T & \mathbf{K}_{wx}^T & \mathbf{K}_{xx} & \mathbf{K}_{x\theta}\\ \mathbf{K}_{u\theta}^T & \mathbf{K}_{v\theta}^T & \mathbf{K}_{w\theta}^T & \mathbf{K}_{x\theta}^T & \mathbf{K}_{\theta\theta}\end{bmatrix},\quad \mathbf{M}=\begin{bmatrix}\mathbf{M}_{uu} & \mathbf{0} & \mathbf{0} & \mathbf{M}_{ux} & \mathbf{0}\\ \mathbf{0} & \mathbf{M}_{vv} & \mathbf{0} & \mathbf{0} & \mathbf{M}_{v\theta}\\ \mathbf{0} & \mathbf{0} & \mathbf{M}_{ww} & \mathbf{0} & \mathbf{0}\\ \mathbf{M}_{ux}^T & \mathbf{0} & \mathbf{0} & \mathbf{M}_{xx} & \mathbf{0}\\ \mathbf{0} & \mathbf{M}_{v\theta}^T & \mathbf{0} & \mathbf{0} & \mathbf{M}_{\theta\theta}\end{bmatrix},\quad \mathbf{H}=\begin{pmatrix}\mathbf{H}_u\\ \mathbf{H}_v\\ \mathbf{H}_w\\ \mathbf{H}_x\\ \mathbf{H}_\theta\end{pmatrix}$$

$$U=\frac{1}{2}\int\int_S\left\{\begin{array}{l}A_{11}\left(\frac{\partial u_0}{\partial x}\right)^2+A_{11}\left(\frac{1}{R}\frac{\partial v_0}{\partial\theta}+\frac{w_0}{R}\right)^2+A_{66}\left(\frac{\partial v_0}{\partial x}+\frac{\partial u_0}{R\partial\theta}\right)^2+\kappa A_{66}\left(\frac{\partial w_0}{\partial x}+\psi_x\right)^2\\ +\kappa A_{66}\left(\frac{\partial w_0}{R\partial\theta}-\frac{v_0}{R}+\psi_\theta\right)^2+2A_{12}\left(\frac{\partial u_0}{\partial x}\right)\left(\frac{1}{R}\frac{\partial v_0}{\partial\theta}+\frac{w_0}{R}\right)+2B_{11}\frac{\partial u_0}{\partial x}\frac{\partial\psi_x}{\partial x}\\ +B_{11}\left(\frac{1}{R}\frac{\partial v_0}{\partial\theta}+\frac{w_0}{R}\right)\frac{\partial\psi_\theta}{R\partial\theta}+2B_{12}\frac{\partial u_0}{\partial x}\frac{\partial\psi_\theta}{R\partial\theta}+2B_{12}\left(\frac{1}{R}\frac{\partial v_0}{\partial\theta}+\frac{w_0}{R}\right)\frac{\partial\psi_x}{\partial x}\\ +2B_{66}\left(\frac{\partial v_0}{\partial x}+\frac{\partial u_0}{R\partial\theta}\right)\left(\frac{\partial\psi_\theta}{\partial x}+\frac{\partial\psi_\theta}{R\partial\theta}\right)+D_{11}\left(\frac{\partial\psi_x}{\partial x}\right)^2+D_{11}\left(\frac{\partial\psi_\theta}{R\partial\theta}\right)^2\\ +2D_{12}\left(\frac{\partial\psi_x}{\partial x}\right)\left(\frac{\partial\psi_\theta}{R\partial\theta}\right)+D_{66}\left(\frac{\partial\psi_\theta}{\partial x}+\frac{\partial\psi_x}{R\partial\theta}\right)^2\end{array}\right\}dS$$

$$\begin{aligned}\mathbf{K}_{uu}=&\int\int\left\{A_{11}\frac{\partial\mathbf{U}^T}{\partial x}\frac{\partial\mathbf{U}}{\partial x}+\kappa A_{66}\frac{1}{R_\alpha^2}\mathbf{U}^T\mathbf{U}+A_{66}\frac{1}{R^2}\frac{\partial\mathbf{U}^T}{\partial\theta}\frac{\partial\mathbf{U}}{\partial\theta}\right\}dS\\&+\int\int\left\{k_{x0}^u\mathbf{U}^T\mathbf{U}\right\}_{|x=0}dS_0+\int\int\left\{k_{x1}^u\mathbf{U}^T\mathbf{U}\right\}_{|x=L}dS_1+\int\int\left\{k_{\theta0}^u\mathbf{U}^T\mathbf{U}\right\}_{|\theta=0}dS_2+\int\int\left\{k_{\theta1}^u\mathbf{U}^T\mathbf{U}\right\}_{|\theta=\varphi}dS_3\end{aligned}$$

$$\mathbf{K}_{uv}=\int\int\left\{A_{66}\frac{1}{R}\left(\frac{\partial\mathbf{U}^T}{\partial\theta}\frac{\partial\mathbf{V}}{\partial x}+\frac{\partial\mathbf{U}}{\partial\theta}\frac{\partial\mathbf{V}^T}{\partial x}\right)+A_{12}\frac{1}{R}\left(\frac{\partial\mathbf{U}^T}{\partial x}\frac{\partial\mathbf{V}}{\partial\theta}+\frac{\partial\mathbf{U}}{\partial x}\frac{\partial\mathbf{V}^T}{\partial\theta}\right)\right\}dS$$

$$\mathbf{K}_{uw}=\int\int\left\{A_{12}\frac{1}{R}\left(\frac{\partial\mathbf{U}^T}{\partial x}\mathbf{W}+\mathbf{W}^T\frac{\partial\mathbf{U}}{\partial x}\right)\right\}dS$$

$$\mathbf{K}_{ux}=\int\int\left\{B_{11}\left(\frac{\partial\mathbf{U}^T}{\partial x}\frac{\partial\mathbf{\Phi}}{\partial x}+\frac{\partial\mathbf{U}}{\partial x}\frac{\partial\Phi^T}{\partial x}\right)+B_{66}\frac{1}{R^2}\left(\frac{\partial\mathbf{U}^T}{\partial\theta}\frac{\partial\Phi}{\partial\theta}+\frac{\partial\mathbf{U}}{\partial\theta}\frac{\partial\Phi^T}{\partial\theta}\right)\right\}dS$$

$$\mathbf{K}_{u\theta}=\int\int\left\{B_{12}\frac{1}{R}\left(\frac{\partial\mathbf{U}^T}{\partial x}\frac{\partial\Theta}{\partial\theta}+\frac{\partial\mathbf{U}}{\partial x}\frac{\partial\mathbf{\Theta}^T}{\partial\theta}\right)+B_{66}\frac{1}{R}\left(\frac{\partial\mathbf{U}^T}{\partial\theta}\frac{\partial\mathbf{\Theta}}{\partial x}+\frac{\partial\mathbf{U}}{\partial\theta}\frac{\partial\mathbf{\Theta}^T}{\partial x}\right)\right\}dS$$

$$\begin{aligned}\mathbf{K}_{vv}=&\int\int\left\{A_{11}\frac{1}{R^2}\frac{\partial\mathbf{V}^T}{\partial\theta}\frac{\partial\mathbf{V}}{\partial x}+\kappa A_{66}\frac{1}{R^2}\mathbf{V}^T\mathbf{V}\right\}dS\\&+\int\int\left\{k_{x0}^u\mathbf{V}^T\mathbf{V}\right\}_{|x=0}dS_0+\int\int\left\{k_{x1}^u\mathbf{V}^T\mathbf{V}\right\}_{|x=L}dS_1+\int\int\left\{k_{\theta0}^u\mathbf{V}^T\mathbf{V}\right\}_{|\theta=0}dS_2+\int\int\left\{k_{\theta1}^u\mathbf{V}^T\mathbf{V}\right\}_{|\theta=\varphi}dS_3\end{aligned}$$

$$\mathbf{K}_{vw}=\int\int\left\{A_{11}\frac{1}{R^2}\left(\frac{\partial\mathbf{V}^T}{\partial\theta}\mathbf{W}+\mathbf{W}^T\frac{\partial\mathbf{V}}{\partial\theta}\right)+\kappa A_{66}\frac{1}{R^2}\left(\frac{\partial\mathbf{W}^T}{\partial\theta}\mathbf{V}+\mathbf{V}^T\frac{\partial\mathbf{W}}{\partial\theta}\right)\right\}dS$$

$$\mathbf{K}_{vx}=\int\int\left\{B_{12}\frac{1}{R}\left(\frac{\partial\mathbf{V}^T}{\partial\theta}\frac{\partial\mathbf{\Phi}^T}{\partial x}+\frac{\partial\mathbf{\Phi}^T}{\partial\theta}\frac{\partial\mathbf{V}}{\partial x}\right)+B_{66}\frac{1}{R}\left(\frac{\partial\mathbf{V}^T}{\partial x}\frac{\partial\mathbf{\Phi}}{\partial\theta}+\frac{\partial\mathbf{\Phi}^T}{\partial x}\frac{\partial\mathbf{V}}{\partial\theta}\right)\right\}dS$$

$$\mathbf{K}_{v\theta}=\int\int\left\{\kappa A_{66}\frac{1}{R}\left(\mathbf{V}^T\mathbf{\Theta}+\mathbf{\Theta}^T\mathbf{V}\right)+B_{11}\frac{1}{R^2}\left(\frac{\partial\mathbf{V}^T}{\partial\theta}\frac{\partial\mathbf{\Theta}}{\partial\theta}+\frac{\partial\mathbf{\Theta}^T}{\partial\theta}\frac{\partial\mathbf{V}}{\partial\theta}\right)+B_{66}\left(\frac{\partial\mathbf{V}^T}{\partial x}\frac{\partial\mathbf{\Theta}}{\partial x}+\frac{\partial\mathbf{\Theta}^T}{\partial x}\frac{\partial\mathbf{V}}{\partial x}\right)\right\}dS$$

$$\mathbf{K}_{ww} = \int\int \left\{ A_{11}\frac{1}{R^2}\mathbf{W}^T\mathbf{W} + \kappa A_{66}\frac{\partial \mathbf{W}^T}{\partial x}\frac{\partial \mathbf{W}}{\partial x} + \kappa A_{66}\frac{1}{R^2}\frac{\partial \mathbf{W}^T}{\partial \theta}\frac{\partial \mathbf{W}}{\partial \theta} \right\} dS$$
$$+ \int\int \left\{ k^w_{x0}\mathbf{W}^T\mathbf{W} \right\}_{|x=0} dS_0 + \int\int \left\{ k^w_{x1}\mathbf{W}^T\mathbf{W} \right\}_{|x=L} dS_1 + \int\int \left\{ k^w_{\theta 0}\mathbf{W}^T\mathbf{W} \right\}_{|\theta=0} dS_2 + \int\int \left\{ k^w_{\theta 1}\mathbf{W}^T\mathbf{W} \right\}_{|\theta=\varphi} dS_3$$

$$\mathbf{K}_{wx} = \int\int \left\{ \kappa A_{66}\left(\frac{\partial \mathbf{W}^T}{\partial x}\mathbf{\Phi} + \frac{\partial \mathbf{W}}{\partial x}\mathbf{\Phi}^T \right) + B_{12}\frac{1}{R}\left(\frac{\partial \mathbf{\Phi}^T}{\partial x}\mathbf{W} + \frac{\partial \mathbf{\Phi}}{\partial x}\mathbf{W}^T \right) \right\} dS$$

$$\mathbf{K}_{w\theta} = \int\int \left\{ \kappa A_{66}\left(\frac{\partial \mathbf{W}^T}{\partial \theta}\mathbf{\Theta} + \frac{\partial \mathbf{W}}{\partial \theta}\mathbf{\Theta}^T \right) + B_{11}\frac{1}{R^2}\left(\frac{\partial \mathbf{\Theta}^T}{\partial \theta}\mathbf{W} + \frac{\partial \mathbf{\Theta}}{\partial \theta}\mathbf{W}^T \right) \right\} dS$$

$$\mathbf{K}_{xx} = \int\int \left\{ \kappa A_{66}\mathbf{\Phi}^T\mathbf{\Phi} + D_{11}\frac{\partial \mathbf{\Phi}^T}{\partial x}\frac{\partial \mathbf{\Phi}}{\partial x} + D_{66}\frac{1}{R^2}\frac{\partial \mathbf{\Phi}^T}{\partial x}\frac{\partial \mathbf{\Phi}}{\partial x} \right\} dS$$
$$+ \int\int \left\{ K^x_{x0}\mathbf{\Phi}^T\mathbf{\Phi} \right\}_{|x=0} dS_0 + \int\int \left\{ K^x_{x1}\mathbf{\Phi}^T\mathbf{\Phi} \right\}_{|x=L} dS_1 + \int\int \left\{ K^x_{\theta 0}\mathbf{\Phi}^T\mathbf{\Phi} \right\}_{|\theta=0} dS_2 + \int\int \left\{ K^x_{\theta 1}\mathbf{\Phi}^T\mathbf{\Phi} \right\}_{|\theta=\varphi} dS_3$$

$$\mathbf{K}_{x\theta} = \int\int \left\{ D_{12}\frac{1}{R}\left(\frac{\partial \mathbf{\Phi}}{\partial x}\frac{\partial \mathbf{\Theta}^T}{\partial \theta} + \frac{\partial \mathbf{\Theta}}{\partial \theta}\frac{\partial \mathbf{\Phi}^T}{\partial x} \right) + D_{66}\frac{1}{R}\left(\frac{\partial \mathbf{\Phi}}{\partial \theta}\frac{\partial \mathbf{\Theta}^T}{\partial x} + \frac{\partial \mathbf{\Theta}}{\partial x}\frac{\partial \mathbf{\Phi}^T}{\partial \theta} \right) \right\}$$

$$\mathbf{K}_{\theta\theta} = \int\int \left\{ \kappa A_{66}\mathbf{\Theta}^T\mathbf{\Theta} + D_{11}\frac{1}{R}\frac{\partial \mathbf{\Theta}^T}{\partial \theta}\frac{\partial \mathbf{\Theta}}{\partial \theta} + D_{66}\frac{\partial \mathbf{\Theta}^T}{\partial x}\frac{\partial \mathbf{\Theta}}{\partial x} \right\} dS$$
$$+ \int\int \left\{ K^\theta_{x0}\mathbf{\Theta}^T\mathbf{\Theta} \right\}_{|x=0} dS_0 + \int\int \left\{ K^\theta_{x1}\mathbf{\Theta}^T\mathbf{\Theta} \right\}_{|x=L} dS_1 + \int\int \left\{ K^\theta_{\theta 0}\mathbf{\Theta}^T\mathbf{\Theta} \right\}_{|\theta=0} dS_2 + \int\int \left\{ K^\theta_{\theta 1}\mathbf{\Theta}^T\mathbf{\Theta} \right\}_{|\theta=\varphi} dS_3$$

$$\mathbf{M}_{uu} = \int\int \left\{ I_0\mathbf{U}^T\mathbf{U} \right\} dS; \quad \mathbf{M}_{vv} = \int\int \left\{ I_0\mathbf{V}^T\mathbf{V} \right\} dS; \quad \mathbf{M}_{ww} = \int\int \left\{ I_0\mathbf{W}^T\mathbf{W} \right\} dS;$$

$$\mathbf{M}_{xx} = \int\int \left\{ I_2\mathbf{\Phi}^T\mathbf{\Phi} \right\} dS; \quad \mathbf{M}_{\theta\theta} = \int\int \left\{ I_2\mathbf{\Theta}^T\mathbf{\Theta} \right\} dS;$$

$$\mathbf{M}_{ux} = \int\int \left\{ I_1\mathbf{U}^T\mathbf{\Phi} + \mathbf{U}\mathbf{\Phi}^T \right\} dS; \quad \mathbf{M}_{v\theta} = \int\int \left\{ I_1\mathbf{V}^T\mathbf{\Theta} + \mathbf{V}\mathbf{\Phi}^T \right\} dS;$$

$$\mathbf{H}_u = \begin{Bmatrix} A^u_{00}, A^u_{01}, \cdots, A^u_{m'0}, A^u_{m'1}, \cdots, A^u_{m'n'}, \cdots, A^u_{MN}, \\ a^1_0, \cdots, a^1_M, a^2_0, \cdots, a^2_M, b^1_0, \cdots, b^1_N, b^2_0, \cdots b^2_N \end{Bmatrix}$$

$$\mathbf{H}_v = \begin{Bmatrix} B^v_{00}, B^v_{01}, \cdots, B^v_{m'0}, B^v_{m'1}, \cdots, B^v_{m'n'}, \cdots, B^v_{MN}, \\ c^1_0, \cdots, c^1_M, c^2_0, \cdots, c^2_M, d^1_0, \cdots, d^1_N, d^2_0, \cdots d^2_N \end{Bmatrix}$$

$$\mathbf{H}_w = \begin{Bmatrix} C^w_{00}, C^w_{01}, \cdots, C^w_{m'0}, C^w_{m'1}, \cdots, C^w_{m'n'}, \cdots, C^w_{MN}, \\ e^1_0, \cdots, e^1_M, e^2_0, \cdots, e^2_M, ef^1_0, \cdots, f^1_N, f^2_0, \cdots f^2_N \end{Bmatrix}$$

$$\mathbf{H}_x = \begin{Bmatrix} D^x_{00}, D^x_{01}, \cdots, D^x_{m'0}, D^x_{m'1}, \cdots, D^x_{m'n'}, \cdots, D^x_{MN}, \\ g^1_0, \cdots, g^1_M, g^2_0, \cdots, g^2_M, h^1_0, \cdots, h^1_N, h^2_0, \cdots h^2_N \end{Bmatrix}$$

$$\mathbf{H}_\theta = \begin{Bmatrix} E^\theta_{00}, E^\theta_{01}, \cdots, E^\theta_{m'0}, E^\theta_{m'1}, \cdots, E^\theta_{m'n'}, \cdots, E^\theta_{MN}, \\ k^1_0, \cdots, k^1_M, k^2_0, \cdots, k^2_M, q^1_0, \cdots, q^1_N, q^2_0, \cdots q^2_N \end{Bmatrix}$$

where

$$\mathbf{U} = \begin{Bmatrix} \cos\lambda_0 x, \cdots, \cos\lambda_0 x\cos\lambda_n\theta, \cdots, \cos\lambda_M x\cos\lambda_N\theta, \\ \chi_1(\theta), \cdots, \chi_1(\theta)\cos\lambda_m x, \cdots, \chi_2(\theta)\cos\lambda_M x, \\ \zeta_1(x), \cdots, \zeta_1(x)\cos\lambda_n\theta, \cdots, \zeta_2(x)\cos\lambda_N\theta, \end{Bmatrix} \mathbf{V} = \mathbf{W} = \mathbf{\Phi} = \mathbf{\Theta} = \mathbf{U}$$